AN ABSTRACT OF THE THESIS OF

DAVID MING-SHIH TAO for the MASTER OF SCIENCE
(Name)   (Degree)

Electrical and
in Electronics Engineering   presented on May 6, 1968
(Major)   (Date)

Title: PERCUSSIVE-WELDED P-N JUNCTIONS IN SILICON

Abstract approved: ███████████████████
James C. Looney

This thesis investigates a way to fabricate P-N junctions by percussive welding. The theoretical basis of percussive welding, design considerations of the apparatus used, and the electrical characteristics of the junctions were the main objectives of this investigation.

P-type silicon wafers and gold wire doped with arsenic as a N-type impurity source were the materials studied. It was found that percussive welding alone gave ohmic contacts. An alloying treatment changed the junctions to rectifying type.

The junction capacitance versus reverse bias voltage relations were studied. From these relations, impurity profiles of a simple alloyed junction and an alloyed percussive-welded junction were obtained. A comparison between the two impurity profiles was given.

Percussive-Welded P-N Junctions in Silicon
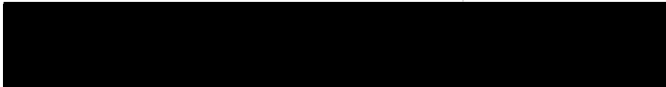
by

David Ming-Shih Tao

A THESIS

submitted to

Oregon State University

in partial fulfillment of
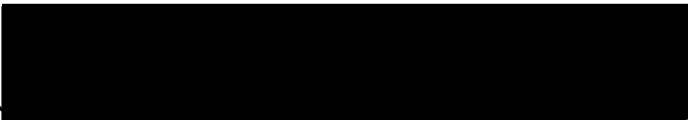the requirements for the
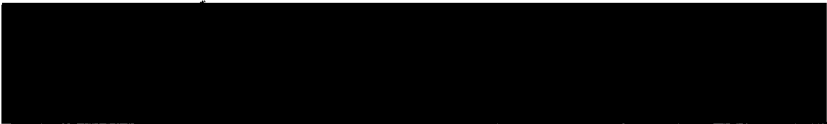degree of

Master of Science

June 1968

APPROVED:

Associate Professor of Electrical and Electronics
Engineering

in charge of major

Head of Department of Electrical and Electronics
Engineering

Dean of Graduate School

Date thesis is presented _____ *May 6, 1968*

Typed by Clover Redfern for _____ David Ming-Shih Tao

ACKNOWLEDGMENT

TABLE OF CONTENTS

LIST OF FIGURES

LIST OF TABLES

PERCUSSIVE-WELDED P-N JUNCTIONS IN SILICON

I. INTRODUCTION

Percussive welding has been utilized for more than a half century. This thesis proposes the method of fabricating P-N junctions in silicon by percussive welding process.

The percussive welding process and the alloying process are actually similar processes. The former has a shorter heat cycle than the latter. It is expected that the percussive welding process can replace the alloying process in fabricating P-N junctions and a junction which has a flat impurity profile will result from the short heat cycle of percussive welding. All these give the motivation of this feasibility study.

Gold wire doped with arsenic as a N-type impurity source and P-type silicon wafers are the materials studied. A welding apparatus which consists mainly of a moving beam and a capacitor discharge circuit has been designed and built. It will be shown that percussive welding alone gives ohmic junction, an alloying treatment changes the junction to rectifying type; and the alloyed percussive-welded junction has an impurity profile the same as the simple alloyed junction.

II. THEORETICAL ASPECTS OF PERCUSSIVE WELDING

If there is a voltage applied to a moving wire approaching a wafer, the air will break down when the field intensity in the gap between the wire and the wafer reaches the air breakdown value. There will be an arc between the wire and the wafer. The arc energy comes from the energy stored in the capacitor of the welding apparatus. The arc generates heat to melt the wire tip and the wafer. The molten wire tip and the molten pool of wafer will finally get in contact with each other as the wire continues to move toward the wafer. A mixture is formed from the two molten materials. As the arc extinguishes the mixture will cool off and start to solidify. A weld between the wire and the wafer is formed by this way. The wire is moving with respect to the wafer during the welding process, so it has the name "percussive welding."

a. Heat Loss of Wafer and Wire

During the arc the wire tip is melted, as is the silicon wafer opposite the wire tip, as shown in Figure 1. The air will break down at a distance of 0.00005 inch for 50 volts (2, p. 63), then for the same air break down field intensity the distance between the wire and the wafer, when arc begins, will be 0.12 mils for 120 volts. This distance gives us some confidence that the molten wafer will be a

Doped gold wire

10 mils

0. 12
mils

Air

Air

d

500 mils

20 mils

Silicon wafer
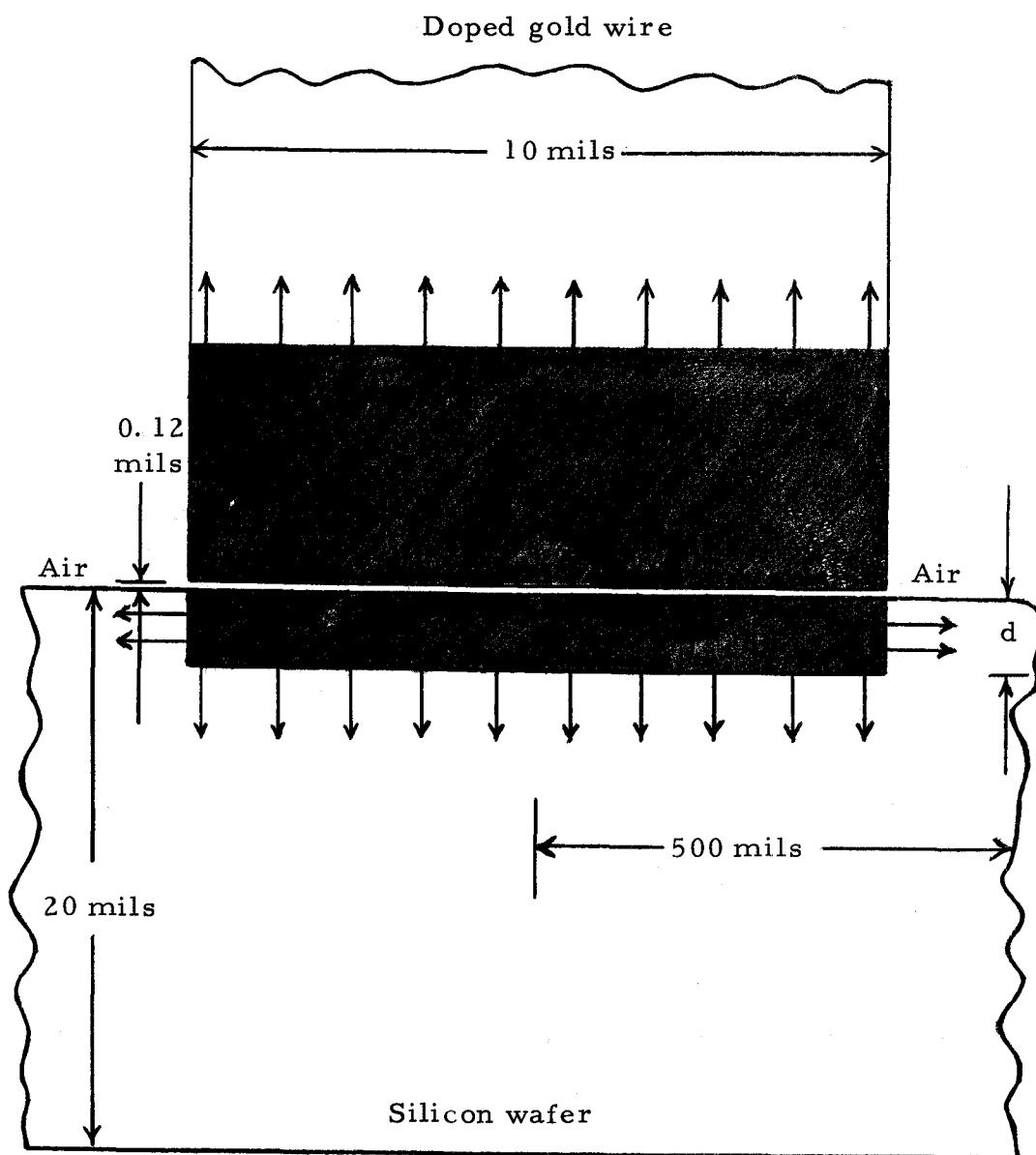
Figure 1. Heat losses of wafer and wire. (Shaded
area for molten zone, not to scale.)

cylinder of ten mils diameter at the very beginning of this process, because the current path can not spread out very much in that short distance, and it is the current and the arc voltage which give the power to melt the wire and the wafer.

The configuration in Figure 1 suggests that convection and radiation losses can be neglected because the wire is surrounded by air, which is a poor heat conductor as compared to gold and silicon. If the radial conduction loss inside the wafer is also neglected, then the heat losses are approximated by considering the conduction loss in the wire which goes upward and the conduction loss in the wafer which goes downward.

The conduction loss in the wire which goes upward can be estimated by considering the heat loss through an area on the surface of a semi-infinite solid (6, p. 147) as

$$\frac{dQ}{dt} = 4.18 \frac{KA\Delta T}{\sqrt{\pi a t}} \quad \text{watts} \tag{1}$$

where:

$\dfrac{dQ}{dt}$ = conduction loss in watts

K = thermal conductivity in (cal./sec. $^{\circ}$C. cm.)

A = area of the surface in (cm.^{2})

ΔT = temperature difference in ($^{\circ}$C.)

a = thermal diffusivity in (cm.^{2}/sec.)

   = (thermal conductivity)/(specific heat)(density)

t = time in (sec.), t = 0 when arc initiates.

For the specific case under consideration for the wire:

K = 0.7 (cal./sec. $^{\circ}$C. cm.)

A = cross-section area of wire (ten mils dia.)

$= (\pi\ 5^2)(2.54/1000)^2$ cm.^{2}

ΔT = 1400 - 25 = 1375°C

a = 1.165 cm.^{2}/sec. for gold.

Substituting all these values into Equation (1) will give

$$\left.\frac{dQ}{dt}\right|_{wire} = \frac{1.06}{\sqrt{t}} \quad \text{watts} \tag{2}$$

An integration of Equation (2) gives the energy lost in the wire

$$Q\big|_{wire} = 2.12\sqrt{t} \quad \text{joules} \tag{3}$$

The conduction loss in the wafer which goes downward can be calculated by using the same Equation (1), but with different values of constants:

K = 0.2 (cal./sec. $^{\circ}$C. cm.)

A = cross-section of molten cylinder

$= (\pi\ 5^2)(2.54/1000)^2$ cm.^{2}

ΔT = 1375°C

a = 0.488 cm.^{2}/sec. for silicon.

Substituting all these values into Equation (1) will give the wafer power loss

$$\frac{dQ}{dt}\bigg|_{wafer} = \frac{0.464}{\sqrt{t}} \quad watts \qquad (4)$$

An integration of Equation (4) gives the energy lost in the wafer

$$Q\big|_{wafer} = 0.928\sqrt{t} \quad joules \qquad (5)$$

Thus the total power loss from Equation (2) and Equation (4) is:

$$\frac{dQ}{dt} = \frac{dQ}{dt}\bigg|_{wire} + \frac{dQ}{dt}\bigg|_{wafer}$$

$$= \frac{1.524}{\sqrt{t}} \quad watts \qquad (6)$$

An integration gives the total energy loss:

$$Q = Q\big|_{wire} + Q\big|_{wafer}$$

$$= 3.048\sqrt{t} \quad joules \qquad (7)$$

Equation (6) and Equation (7) give the power and energy heat loss of wafer and wire.

b. Relation Among Arc Duration, Wire Melt-back and Wafer Melt-in

The welder capacitor C discharge circuit is a RLC series

circuit. The resistance of the discharge circuit R is adjusted such that the discharge circuit is critically damped. The inductance L is the intrinsic self inductance of the welder capacitor discharge circuit. When arc initiates, the arc will have constant voltage V_a which acts like a battery in the discharge circuit. Then the equation describing the discharging current is;

$$0 = V_a + Ri(t) + L\frac{di(t)}{dt} + \frac{\int_0^t i(t)dt}{C} - V_c \tag{8}$$

Where V_c is the initial capacitor voltage, which is a constant. Taking the Laplace transform of Equation (8) gives

$$\frac{V_c - V_a}{S} = Ri(S) + LSi(S) + \frac{i(S)}{CS}$$

or

$$i(S) = \frac{C(V_c - V_a)}{LCS^2 + CRS + 1}$$

For critical damping, set the denominator equal to zero and solve for two identical roots

$$C^2 R^2 = 4(LC)(1)$$

or

$$L = \frac{R^2 C}{4} \tag{9}$$

Then

$$i(S) = \frac{C(V_c - V_a)}{\frac{R^2 C^2}{4} S^2 + CRS + 1}$$

$$= \frac{4(V_c - V_a)}{R^2 C} \left[\frac{1}{(S + \frac{2}{RC})^2} \right] \tag{10}$$

Taking the inverse Laplace transform of Equation (10) gives

$$i(t) = \frac{4(V_c - V_a)}{R^2 C} (t) \left[e^{-\frac{2}{RC} t} \right] \tag{11}$$

The instantaneous power supplied to the arc is Equation (11) multiplied by V_a, which is (7, p. 3)

$$Pa = [4V_a(V_c - V_a)/R^2 C][t e^{-2t/RC}] \quad \text{watts} \tag{12}$$

where

V_a = arc voltage in volts

V_c = initial capacitor voltage in volts

R = discharge circuit resistance in ohms

C = capacitance of the capacitor to be discharged, in farads.

An integration of Equation (12) gives the energy supplied to the arc: (7, p. 3)

$$E_a = CV_a(V_c-V_a)[1-(1+2t/RC)e^{-2t/RC}] \quad \text{joules} \quad (13)$$

For the specific case considered, $C = 240$ micro farads; $V_a = 15$ volts (assumed); $V_c = 120$ volts; $R = 0.04$ ohms. Substituting these values into Equation (12) and Equation (13) will give:

$$P_a = 1.64 \times 10^{10}t \, e^{-10^6 t/4.8} \quad \text{watts} \quad (14)$$

$$E_a = 0.378[1-(1+10^6 t/4.8)e^{-10^6 t/4.8}] \quad \text{joules} \quad (15)$$

Table 1 on page 12 gives the relation between arc duration, wire melt-back and wafer melt-in. Equation (15) and Equation (7) are used to obtain values for E_a and Q. The difference $E_a - Q$ is Q_m, that is, the total melting energy. The amount of Q_m which goes to the wire can be calculated by considering the parallel paths of heat conduction in the wire and in the wafer[1] as:

$$Q_{m,wire} = Q_m \frac{\sqrt{a_{Si}}/K_{Si}}{\sqrt{a_{Si}}/K_{Si} + \sqrt{a_{Au}}/K_{Au}} \quad (16)$$

If numerical values are used, Equation (16) will give:

---

[1] Refer to Equation (1).

$$Q_{m,wire} = 0.695Q_m \qquad (17)$$

The rest of Q_m will go to wafer:

$$Q_{m,wafer} = 0.305Q_m \qquad (18)$$

Figure 2 gives a plot of melting energy versus volume being melted for the convenience in evaluating column 7 and column 8 in Table 1. Figure 2 is based on the relation:

(melting energy) = (volume)(density)[(specific heat)(melting point
- room temperature)+(latent heat of fusion)] (19)

Columns 9 and 10 in Table 1 are obtained by dividing columns 7 and 8 by $25\pi(\text{mil})^2$, assuming no feathered tip on the wire and a cylindrical molten portion in the wafer. If the arc duration is 2.5 milli-seconds, then a wire melt-back of 36.475 mils can be found by interpolation from Table 1.

The molten wire tip may have the shape of a sphere due to sur-face tension. The cylinder of 10 mils diameter and 36.475 mils in height will have the same volume as a sphere of 8.8 mils in radius. The shrinkage in length of the wire tip will be:

$$36.475 - 2 \times 8.8 = 18.875 \text{ mils} \qquad (20)$$

During the actual experiment a tolerance of 25 mils is used rather than 18.875 mils in order to give more molten material to wet the surface so that a mechanically strong weld will result.

If the arc duration (t_a) can be controlled definitely then the
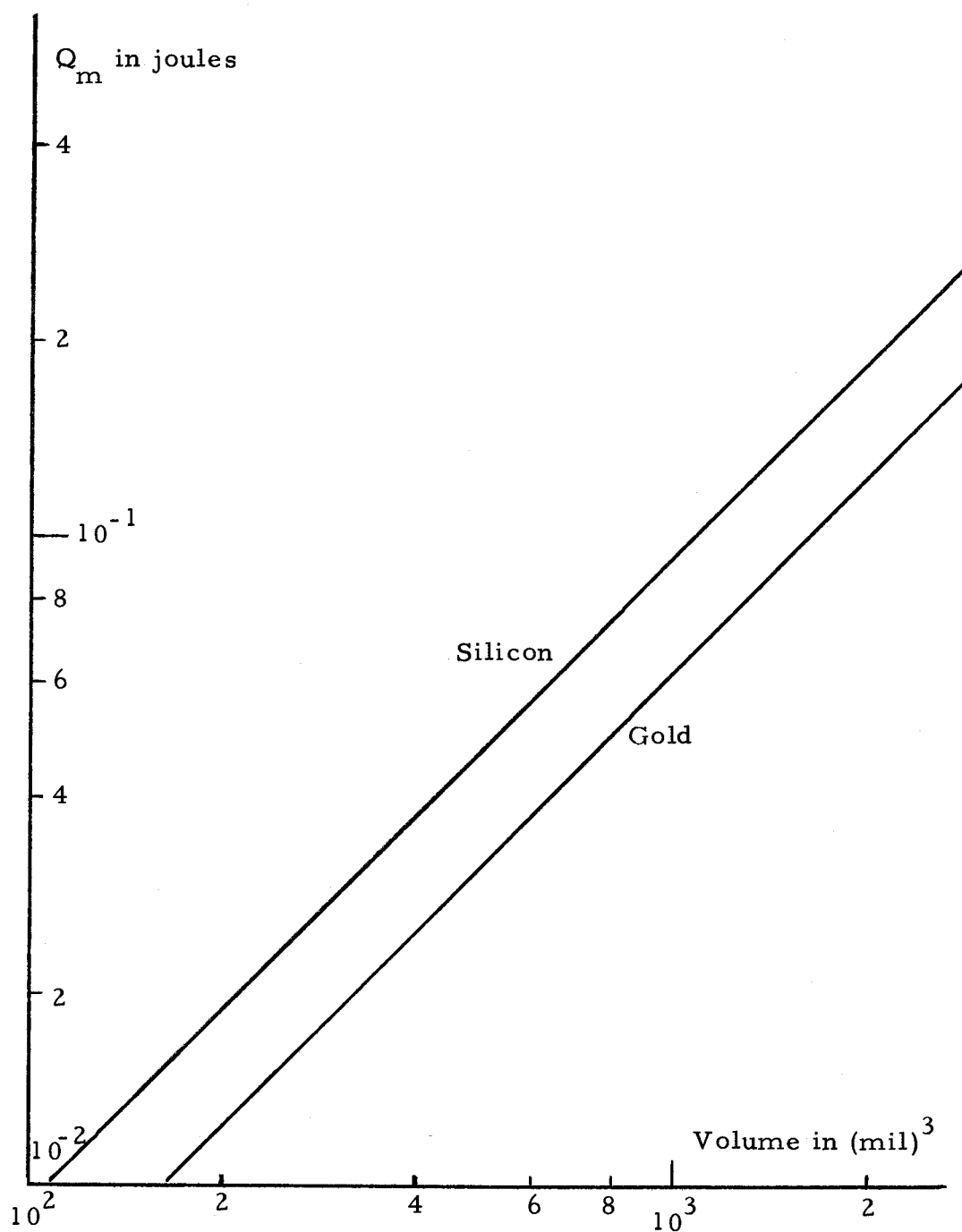
Figure 2.   Energy required to melt a specific volume of material from room temperature.

Table 1. Relation among arc duration, wire melt-back and wafer melt-in.

sec Arc duration=t_a	joules E_a	joules Q	joules $E_a-Q=Q_m$	joules $Q_{m,wire}$	joules $Q_{m,wafer}$	$(mil)^3$ $V_{Au}=V_{wire}$	$(mil)^3$ $V_{Si}=V_{wafer}$	(mil) Wire melt-back	(mil) Wafer melt-in
10^{-5}	0.232	0.00965	0.22235	0.1540	0.0678	2500	720	31.80	9.17
2×10^{-5}	0.348	0.01365	0.33435	0.2320	0.1020	3700	1100	47.10	14.00
4×10^{-5}	0.378	0.01930	0.35870	0.2490	0.1090	4000	1180	51.00	15.00
6×10^{-5}	0.378	0.02360	0.35440	0.2460	0.1080	3950	1150	50.40	14.65
8×10^{-5}	0.378	0.02730	0.35070	0.2440	0.1070	3900	1150	49.70	14.65
10^{-4}	0.378	0.03048	0.34752	0.2420	0.1060	3850	1140	49.00	14.50
2×10^{-4}	0.378	0.04300	0.33500	0.2330	0.1020	3750	1100	47.80	14.00
4×10^{-4}	0.378	0.06096	0.31704	0.2200	0.0966	3550	1040	45.20	13.25
6×10^{-4}	0.378	0.07480	0.30320	0.2110	0.0925	3350	990	42.60	12.60
8×10^{-4}	0.378	0.08640	0.29160	0.2020	0.0888	3250	960	41.40	12.20
10^{-3}	0.378	0.09650	0.28150	0.1950	0.0858	3150	920	40.10	11.70
2×10^{-3}	0.378	0.13650	0.24150	0.1680	0.0736	2700	790	34.40	10.10
4×10^{-3}	0.378	0.19300	0.18500	0.1285	0.0565	2050	610	26.10	7.77
6×10^{-3}	0.378	0.23600	0.14200	0.0986	0.0433	1580	460	20.10	5.86
8×10^{-3}	0.378	0.27300	0.10500	0.0730	0.0320	1170	340	14.90	4.33
10^{-2}	0.378	0.30480	0.07320	0.0510	0.0223	820	235	10.45	3.00
2×10^{-2}	0.378	0.43000	Negative						
4×10^{-2}	0.378	0.60960	Negative						
6×10^{-2}	0.378	0.74800	Negative						
8×10^{-2}	0.378	0.86400	Negative						
10^{-1}	0.378	0.96500	Negative						

wafer melt-in and wire melt-back can be controlled precisely. The fact is that the arc duration is a function of grease action, (grease is applied on stop to prevent the beam from bouncing) beam approaching velocity, circuit inductance, capacitance and charging voltage (4, p. 18). Theoretically it is possible to get good control of the factors mentioned above except the grease action. So it is actually not possible to have the same arc duration every time even with every manageable factor unchanged.

c. Arc Duration Limits to Have a Weld

Figure 3 is a plot of Equation (14) and Equation (6). The area under P_a curve represents energy supplied, the area under dQ/dt curve represents energy lost. $P_a > dQ/dt$ indicated that the wire and wafer are heating up; $P_a < dQ/dt$ means that wire and wafer are cooling off.

Figure 4 is a semi log plot of Figure 3 in order to find when $P_a = dQ/dt$. It is found when $t = 37.5$ micro-seconds $P_a = dQ/dt$ in Figure 4.

From Figure 3 it is obvious that as long as the arc duration is longer than 37.5 micro-seconds the heating up region has passed, which gives a lower limit of arc duration because the wire and the wafer are expected to gain enough heat to become melted.

The cooling off rate of the wire and wafer is very slow as
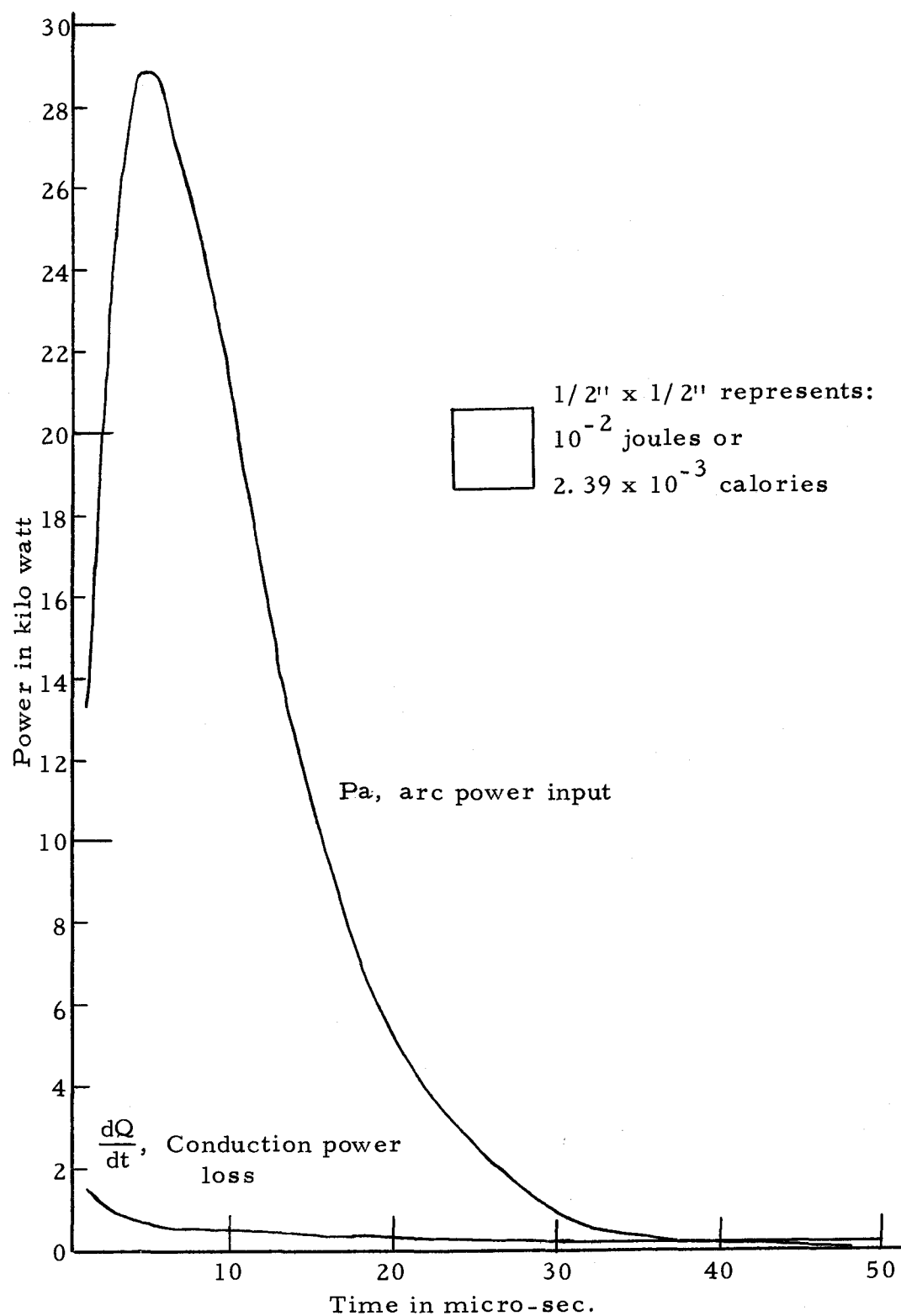
Figure 3. Arc power and conduction power loss of wire and wafer in linear scale.
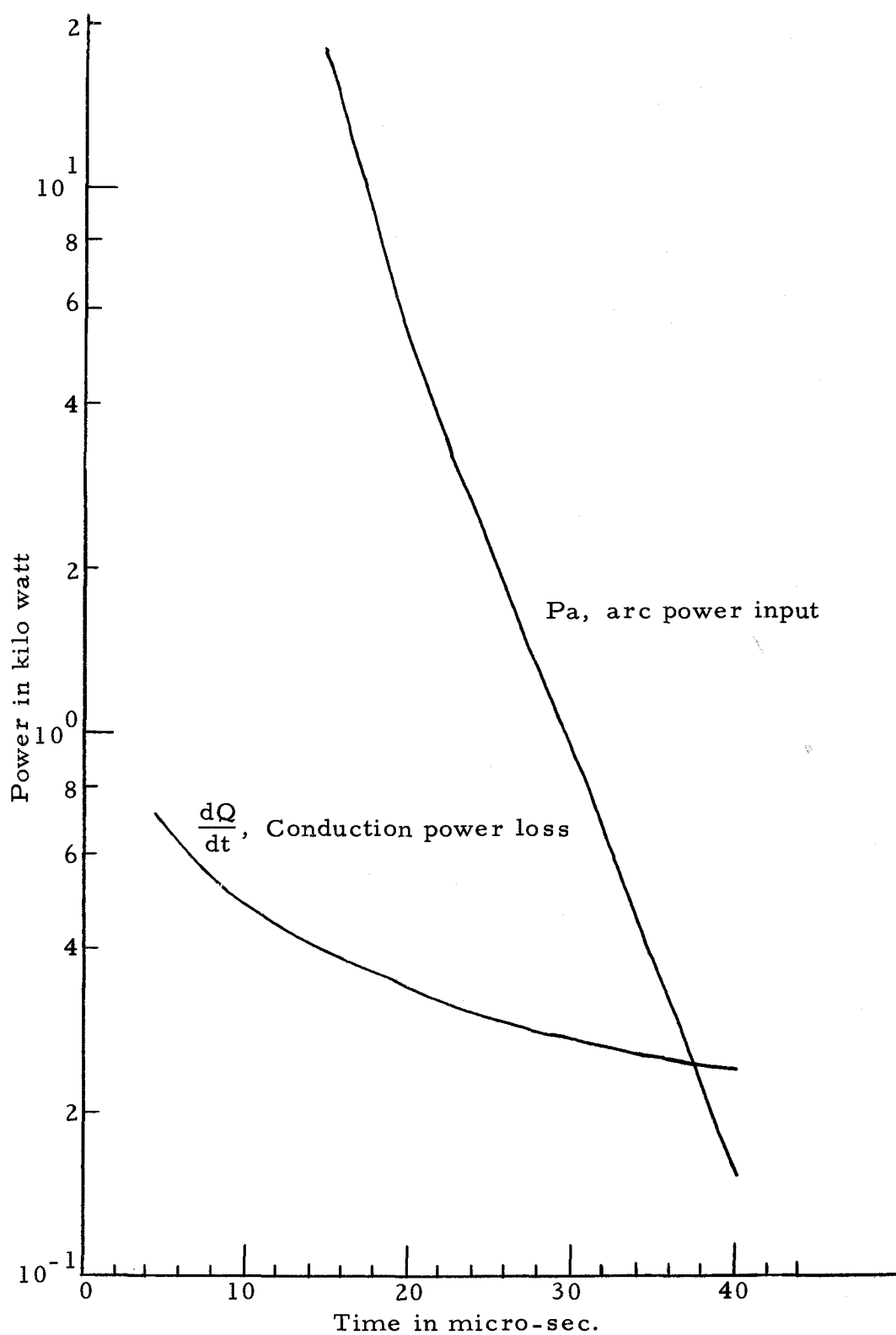
Figure 4. Arc power and conduction power loss of wire and wafer in semi log scale.

compared to the heating up rate, which is quite obvious in Figure 3,

yet there will be an instant that the total supplied energy E_a will

equal the total energy loss Q. Figure 5 is a plot of E_a and Q

as a function of arc duration. All data are in Table 1. From Figure

5, when the arc duration is 1.5×10^{-2} seconds E_a and Q will be

equal, from that instant on Q will be greater than E_a; no melt-

ing energy Q_m will be available. This consideration will give an

upper limit of arc duration of 1.5×10^{-2} seconds or 15 milli-seconds,

because it is desired that the wire and wafer are liquid when they join

together.

An arc duration range is thus determined to be between 37.5

micro-seconds and 15 milli-seconds, which are the limits to form a

weld.

Energy in joules

6

4

2

10^{-1}

8

6

4

2

10^{-2}

8

6

4

2

10^{-3}

E_a, arc energy input

Q, conduction loss

Arc duration in sec.

10^{-5} 2   4   6   8 10^{-4} 2   4   6   8 10^{-3} 2   4   6   8 10^{-2} 2   4   6   8 10^{-1}
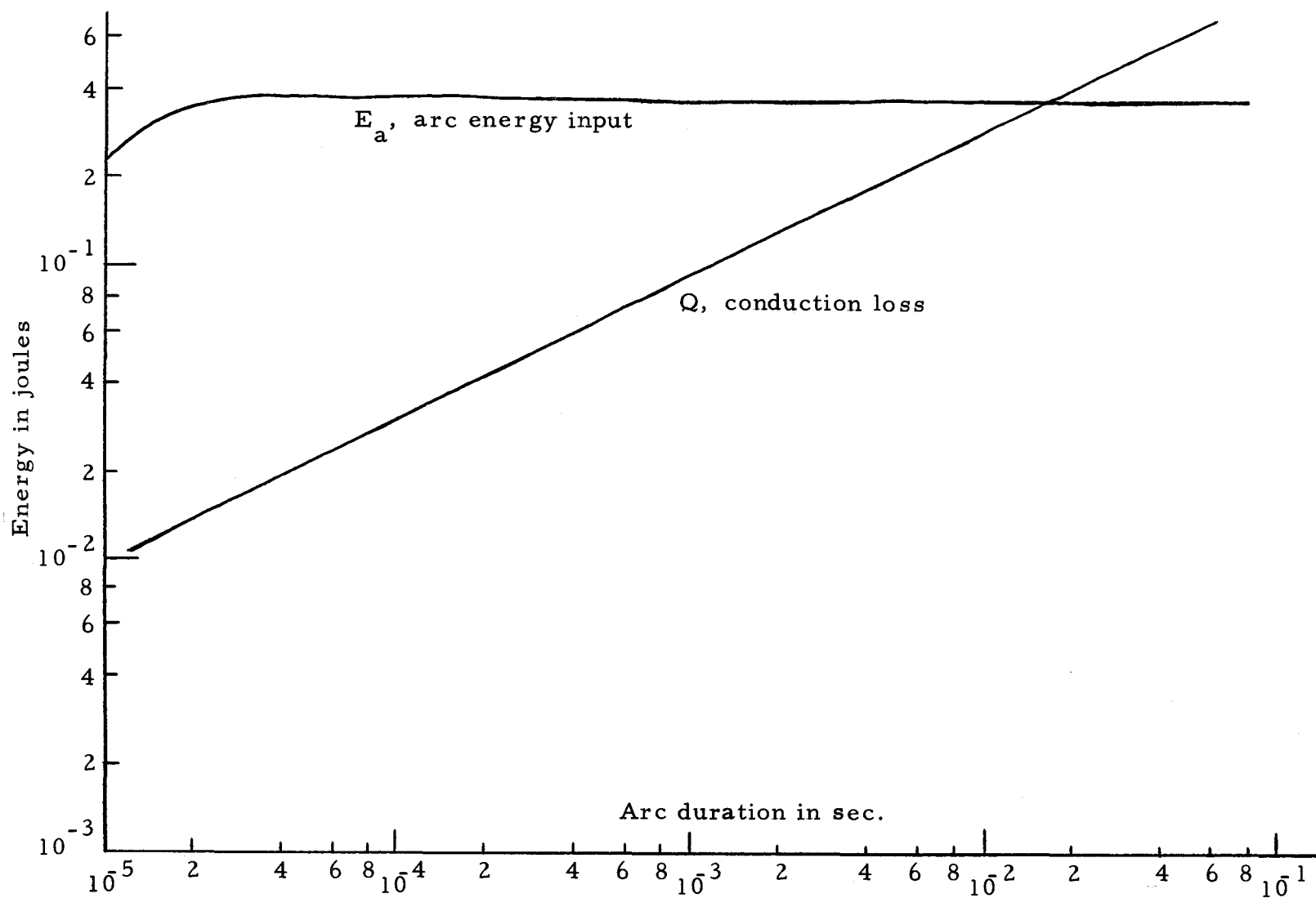
Figure 5.   Arc energy, conduction loss as a function of arc duration.

17

III. APPARATUS DESIGN

In order to perform the percussive welding process, an apparatus had to be built to satisfy the following requirements:

1. A moving part coming toward a stationary part with adjustable approaching speed.

2. Movable wafer holder which will give adjustable position of the wafer with respect to the wire tip in order to give tolerance for the wire tip shrinkage in length.

3. Proper ways to hold wafer and wire firmly in position and provide good electrical connections to them.

4. A rectifier is needed to charge up a big capacitor and then let the capacitor discharge through a low resistance circuit.[2]

Figure 6(a) and (b) show the apparatus which consists of a spring-loaded aluminum beam capable of moving toward a wafer holder and a stop which are under one end. The wafer holder and stop are threaded 40 turns to one inch which gives an adjustment of 25 mils per turn. A vacuum system will hold the wafer on the holder through its hollow interior and small holes on top. The wafer holder and the base together provide electrical contact to the wafer. A

---

[2] Low resistance will minimize the energy dissipation during discharge.
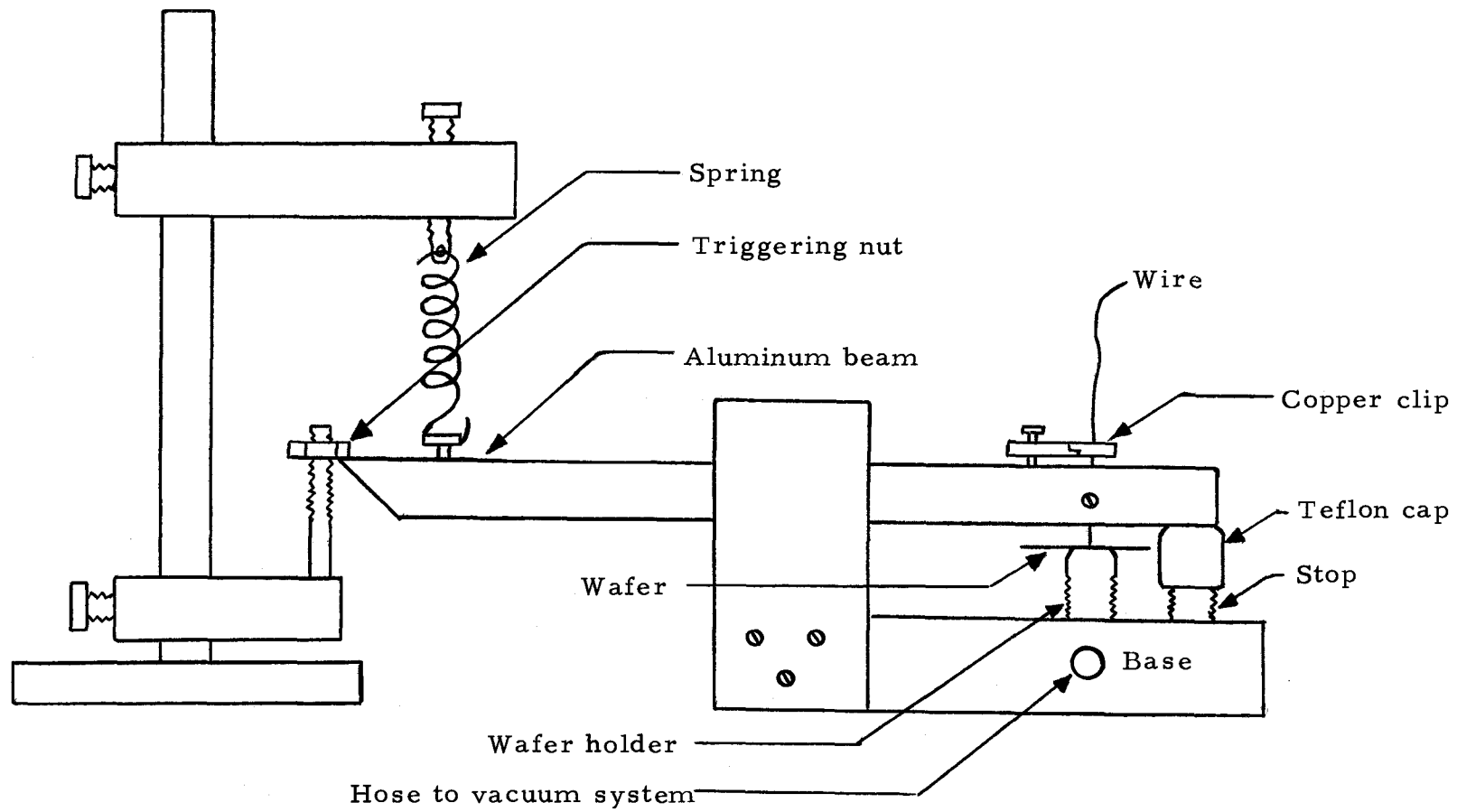
Figure 6(a). Various parts of the welding apparatus.

copper clip is used to hold the wire which goes through a vertical small hole in the beam; the clip provides electrical contact to the wire. A horizontal threaded opening which meets the vertical opening where wire is inserted can be used to lock the wire in by using a screw. A teflon cap is placed on the stop to prevent an undesired arc between the beam and the stop. Triggering of the beam can be adjusted by moving the nut up or down, changing the initial angular displacement of the beam. The spring elongation and thus the spring tension can be adjusted by the screw attached to the spring.
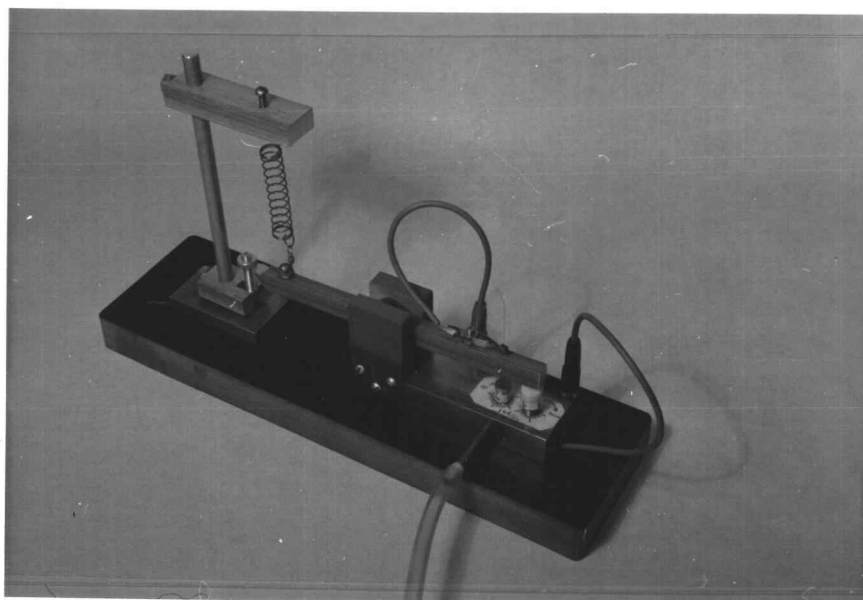
Figure 6(b). The welding apparatus used.

Equation (21) describes the approaching velocity of the wire tip:[3]

---

[3] For derivation see Appendix I (a).

$$\frac{V_{wf}}{r_w} = \frac{1}{4} \sqrt{\frac{K}{I}} \sqrt{\theta_0 r_S (2X_0 + \theta_0 r_S)} \tag{21}$$

where:

V_{wf} = wire tip final approaching speed in (inch/sec.)

r_w = radius of rotation of wire tip in inch

K = spring stiffness in ounch per inch

I = moment of inertia of the beam in slug-inch^2

θ_0 = initial angular displacement of the beam in radian

r_S = moment arm of spring force in inch

X_0 = initial elongation of spring in inch.

This formula can give an estimation of the wire tip approaching speed. In the apparatus used, a 1/2" x 3/8" x 8" aluminum beam pivoted at the center with ball bearings to reduce friction will have a moment of inertia of 0.0242 slug-in^2. [4] A spring of 14 oz/in stiffness was used. The wire tip rotating radius was three inches, and the moment arm of the spring force was three inches. If the initial angular displacement of the beam is 1/6 radian, and initial elongation of the spring is one inch, then a wire tip final approaching speed close to 20 inches per second can be obtained.

There is quite a difference between the wire tip final approaching speed and the average speed the wire tip travels during the arc,

---

[4] For calculation see Appendix I (b).

because the latter is affected mainly by the vacuum grease applied on the stop.

The electrical circuit involved is shown below. Thick wires were used for connection to have low resistance. Ten 24 micro farad electrolytic capacitors were used to build the 240 micro farads capacitance. A variac which could set up to 220 volts and a selenium rectifier were used to supply the d. c. power required to charge up the capacitors. The three kilohms resistor was used to limit the charging time constant. A d. c. voltmeter was used to read the voltage across the capacitors.
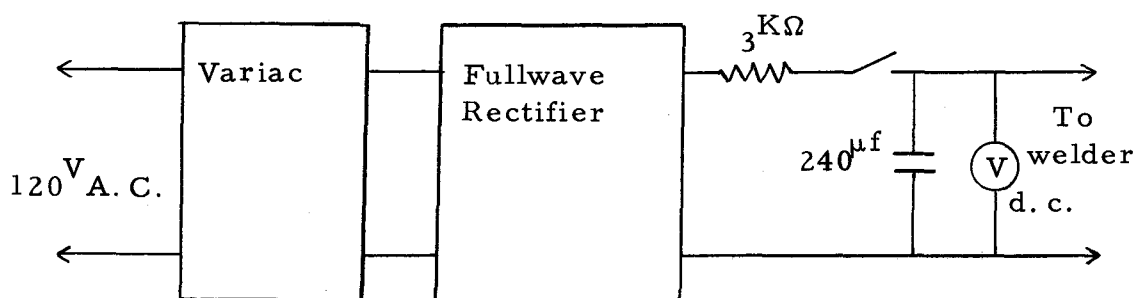
Figure 7. Electrical circuit in the welding apparatus.

IV. EXPERIMENTAL PROCEDURES

a. Procedure to Make a Percussive-welded Junction and an Alloyed Percussive-welded Junction

(i) Percussive-welded Junction

A P-type silicon wafer of 1.2 ohm-cm. resistivity 21 mils thickness and about one inch diameter was used during the process. No grease or dirt including finger prints on the surface of the wafer was allowed. The wafer was etched in CP-5 to clean the surface if necessary. A hydrofluoric acid bath of two minutes to take off silicon oxide followed by a lapping with #600 grit lapping powder, was required to make the wafer surface ready for a weld. Before making the weld, several ohmic alloyed contacts are made on the fringe of the wafer so that there will be no point contact problem involved later on. This is done by alloying 99% Al 1% B dots of 15 mils diameter inside a strip heater at about 650°C, with a forming gas atmosphere. A check with the transistor curve tracer to show that between two ohmic dots there was a negligible resistance gave confidence in this process. Then a short bath in CP-5 was needed just long enough to clean the surface, five seconds would be long enough because a lapped rough surface is better for welding than a mirror finished one. In order that the back side of the wafer will make better contact with the wafer holder, it was copper plated by using a mixture of five parts

saturated $CuSO_4$ aqueous solution and one part concentrate hydrofluoric acid by volume. This plating was stripped off with nitric acid after the weld had been made.

The wire used was 99.9% gold wire doped with 0.1% arsenic of 10 mils diameter. The wire tip was cut into a chisel tip of approximately 45 degrees.

The 240 micro-farad capacitor of the welding apparatus was charged up to 120 volts, the trigger nut was three turns from top. A spring of 14 oz/in stiffness was used. A wire tip melt back of 25 mils[5] was given by raising the wafer holder 25 mils (one turn of the wafer holder). A thin layer of high vacuum grease is applied on the stop to prevent the beam from bouncing. Finally, the beam was let loose by moving the trigger nut which made the weld. A scissors was used to cut the wire after the weld was made.

(ii) Alloyed Percussive-welded Junction

Another heat cycle, by alloying the percussive-welded junction made previously inside a strip heater, was performed in this process. As a comparison to the straight alloying process, dots cut off from the same wire were placed on top of the same type of wafer laying alongside the percussive-welded junction inside the strip heater. The

---

[5] Refer to Equation (20).

strip heater was heated to 482°C for about one minute at a forming gas flow rate of 1.6 SCFH.

A CP-5 etching process was used to clean the surface before mounting on transistor curve tracer to judge the character of the junction.

b. Procedure to Get Metallurgical Observation Samples of the Junctions

In order to judge the similarity and difference among different junctions three samples were made from (1) percussive-welded junctions, (2) alloyed percussive-welded junctions, and (3) simple alloyed junctions, all of them using the same materials.

The samples were mounted in wax on microscope slides, and cut with a diamond saw close to the junction. Then they were lapped with #600 grit powder first and 0.3 micron powder to a final finish. Pictures were taken under a 600 x magnification metallurgical microscope later on.

c. Procedure Used to Obtain Arc Voltage and Arc Current Traces

The arc voltage and arc current wafeforms all happen within several milli seconds in the experiment. A Tektronix type 564 storage scope with a dual trace input was used to store the waveforms. The traces were obtained using the procedure as given in section

IVa(i). A percussive-welded junction was performed with the additional change as shown in Figure 8 for hooking up the probes.
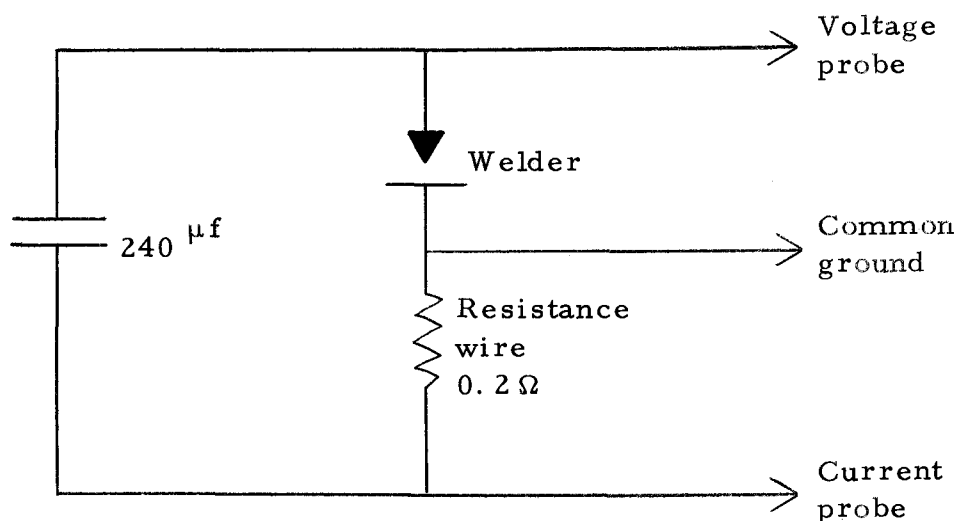
Figure 8. Voltage probe and current probe connection.

A piece of resistance wire of 0.2 ohms resistance was connected in series with the welder discharge circuit so that the voltage waveform across it was the same as the current waveform passing through the arc. The current scale was the voltage scale on the scope divided by 0.2 ohms. The scope was in stored display, chopped mode, internal triggering source and single sweep scanning.

Pictures were taken by using Tektronix C-12 camera mounted on a scope.

d. Junction Capacitance Measurement

When a junction has already been made, the impurity profile of this junction can be known through junction capacitance versus

reverse bias variation measurements.

The junction capacitances of three simple alloyed junctions and three alloyed percussive-welded junctions all made from the same materials were measured by using a Boonton Electronics capacitance bridge model 75 C in order to give the impurity profiles of these junctions.

As long as the leakage resistance of the junction capacitance was greater than one kilohm, the bridge gave a satisfactory reading.

A measuring frequency of five hundred kilocycles and ten millivolts (r.m.s.) signal level was used. The bias voltages applied to the junctions ranged from 2.8 volts (reverse) to 0.2 volts (forward). Outside this range sometimes the junction capacitance became too leaky, that made the measurement impossible. A bias voltage variation step of 0.2 volts was used.

Areas of junctions were different, so average among junction capacitances obtained at the same bias voltage was not made.

All the data obtained are in Appendix II. The impurity profiles evaluated are in section V d .

V. EXPERIMENTAL RESULTS AND EXPLANATIONS

a. Electrical Characteristics of Percussive-welded Junctions and Alloyed Percussive-welded Junctions

Figure 9 shows the ohmic characteristic of a percussive-welded junction. The resistance of this welded junction is 100 ohms, which is different from weld to weld. The resistance of a welded junction depends on the resistivity of the bulk wafer, the distance between the weld and the ohmic contact on wafer, the geometry of the weld and the thickness of the wafer.

Figure 10 shows the rectifying characteristic of the alloyed percussive-welded junction.

The following explanation is believed to give the reason why an additional alloying heat cycle is needed to change the electrical characteristic of a welded junction from ohmic to rectifying.

Figure 11 (a) shows there is a thin layer of frozen alloy of gold and silicon formed during the welding process. Since the gold wire is highly doped with N-type arsenic as compared to the P-type silicon, the frozen alloy is N-type. The P-N junction is therefore between the P-type silicon wafer and the N-type frozen alloy. But when the alloy solidified during the welding process, the wire was moving downward giving a mechanical disturbance to the crystal forming process. And besides the gold wire is polycrystalline in structure, thus
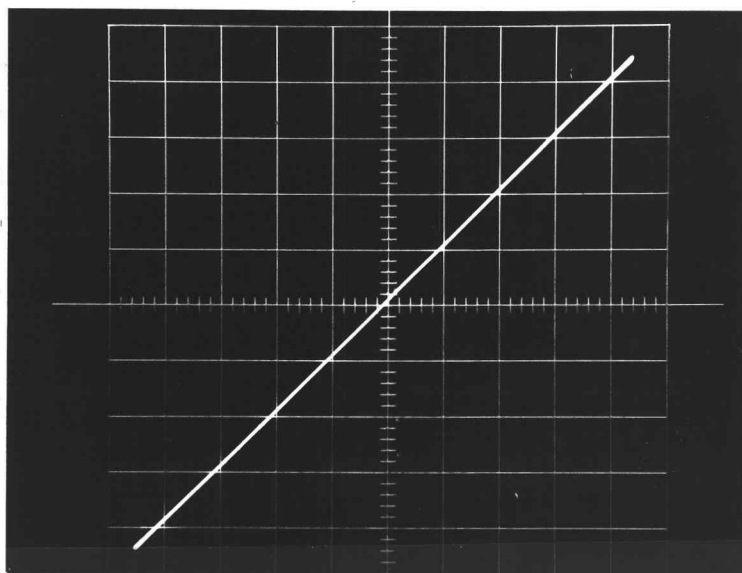
Figure 9.   Ohmic percussive-welded junction characteristic.
            (Horizontal: 0. 1 volt/div.)
            (Vertical: 1 milli-amp. /div.)

Figure 10.   Rectifying alloyed percussive-welded junction
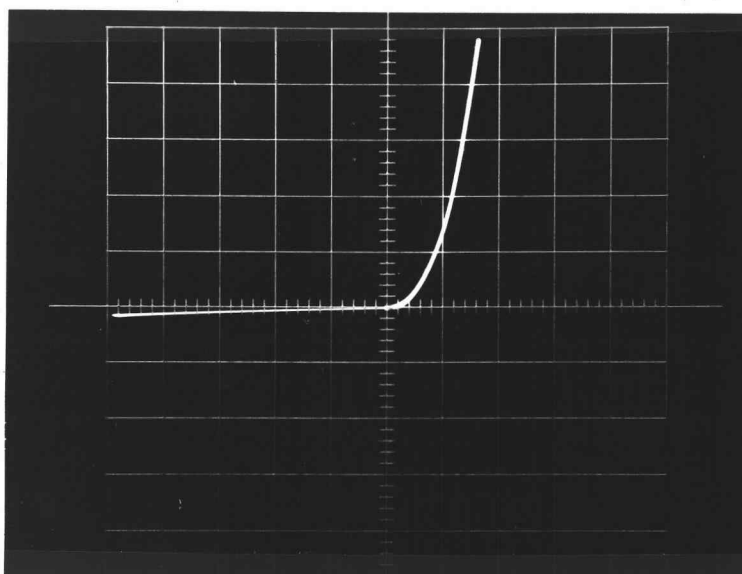   characteristic.
             (Horizontal: 0. 5 volt/div.)
             (Vertical: 0. 5 milli-amp. /div.)

Gold wire doped with N-type arsenic

Thin layer of N-type poly-crystalline gold silicon alloy

P-N junction

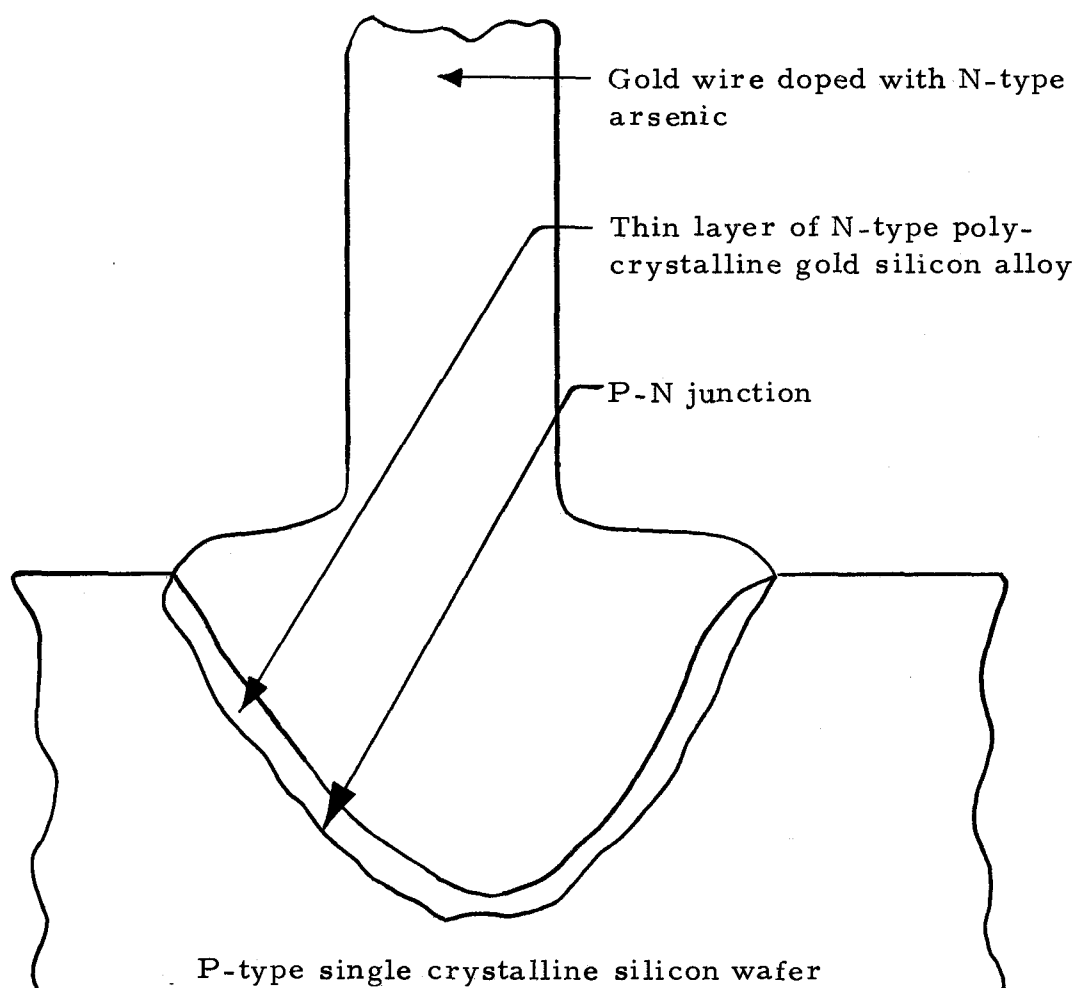P-type single crystalline silicon wafer

Figure 11(a).   Thin layer of gold silicon alloy after welding.

the frozen alloy is polycrystalline in structure. The P-N junction is between the single crystal P-type silicon and the polycrystal N-type alloy, and thus gives an ohmic characteristic as shown in Figure 9.

Figure 11 (b) shows the situation after the alloying process. When the alloying temperature was raised to 482°C, about 112°C above the eutectic point of gold silicon alloy, (3, p. 232) the alloy melted, then as the temperature dropped below the eutectic point, the molten alloy started to freeze again from both the gold wire side and the silicon wafer side toward the liquid-phase molten alloy. Since there was no mechanical disturbance this time, they met at the dotted line in Figure 11 (b). The dotted line is the boundary between single crystal and polycrystal. The crystal which grows from the gold wire side is polycrystalline. The crystal which grows from the silicon wafer side is single crystalline. After the alloying process the P-N junction is now between the single crystal P-type wafer and the single crystal N-type alloy, that gives rectifying characteristics as shown in Figure 10.

While alloying the welded junction, dots cut off from wire tips were put on the same type of wafer as used in the welding process. It was then laid alongside the weld in the strip heater as described in section IV a (ii). When the temperature went up to 482°C, the welded junction started to melt, but nothing happened between the dots and the wafer. This proves that there is some alloy in the welded

N-type polycrystalline alloy

N-type single crystalline alloy
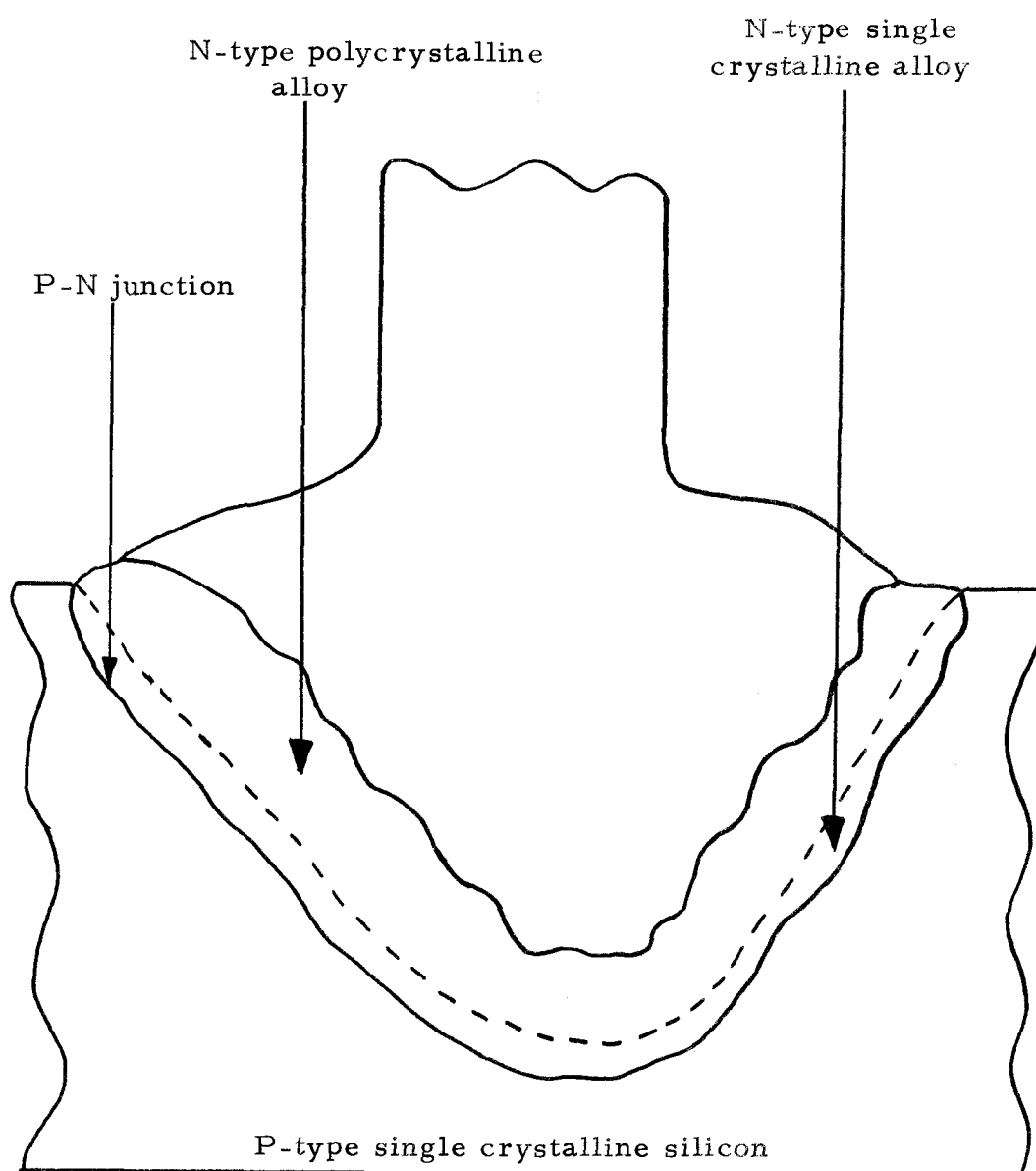
P-N junction

P-type single crystalline silicon

Figure 11(b).   Thin layer after alloying.

junction, because the alloy gives a lower melting point than either the gold or the silicon. The existence of this alloy supports the above explanation of the junction electrical characteristics.

b. Metallurgical Observations of the Junctions

Figure 12 shows the sharp edge boundary of an ohmic percussive-welded junction. The thin layer of polycrystalline alloy is so thin, that it can hardly be seen under 600X magnification. However a close examination under a microscope shows a fine black line between the yellow gold and the grey silicon. The line may not be continuous, but just a tiny spot of this ohmic polycrystalline structure is enough to change the junction electrical characteristic from rectifying to ohmic, because a resistor in parallel with a diode is essentially resistive in character.

Figure 13 and Figure 14 show the zigzag boundaries of a rectifying alloyed-percussive welded junction and a rectifying simple alloyed junction respectively. The zigzag boundaries are due to the longer alloying heat cycle which gives a better chance for the gold and the silicon to mix with each other.

c. Arc Voltage and Arc Current Traces

Figure 15 (a) is an experimental verification of the predicted relation between arc voltage and arc current waveforms as shown in
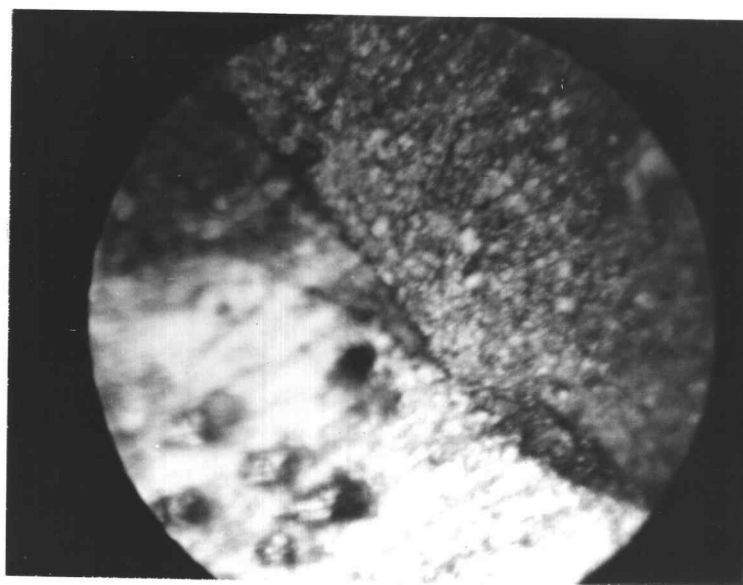
Figure 12. An ohmic percussive-welded junction cross-
section. (The lower-left brighter portion is
gold wire; the upper-right darker portion is
silicon wafer. There is a sharp edge bound-
ary between gold and silicon). 600 x magni-
fication.
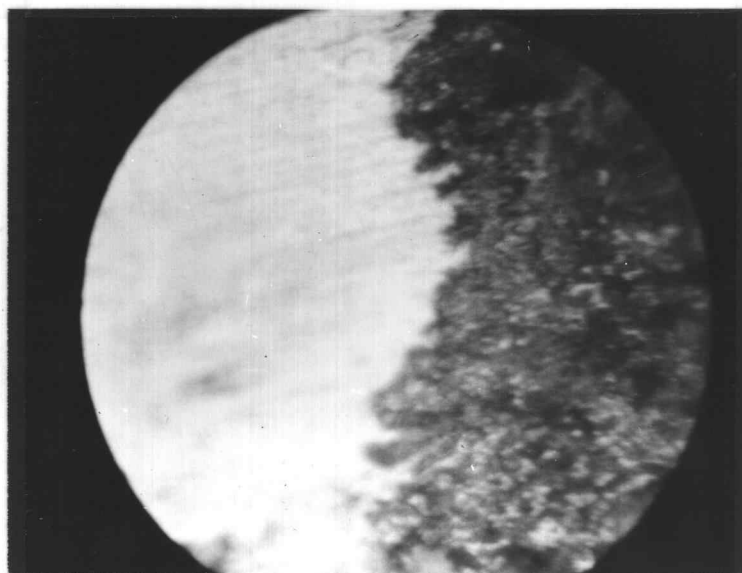
Figure 13. A rectifying alloyed percussive-welded junction
cross-section. (The left, brighter portion is
gold wire; the right, darker portion is silicon
wafer. There is a zigzag edge boundary between
gold and silicon). 600 x magnification.

Figure 14.   A rectifying simple alloyed junction cross-section.
(The upper-left, brighter portion is gold wire;
the lower-right, darker portion is silicon wafer.
There is a zigzag edge boundary between gold and
silicon).   600 x magnification.

Figure 15 (a).   Arc voltage and arc current.   (The upper
trace is arc voltage waveform with a vertical
scale of five volts/div.   The lower trace is
arc current waveform with a vertical scale
of ten amps./div.   The horizontal time scale
is 0. 5 milli-sec./div.).

Figure 15 (b) (2, p. 59).

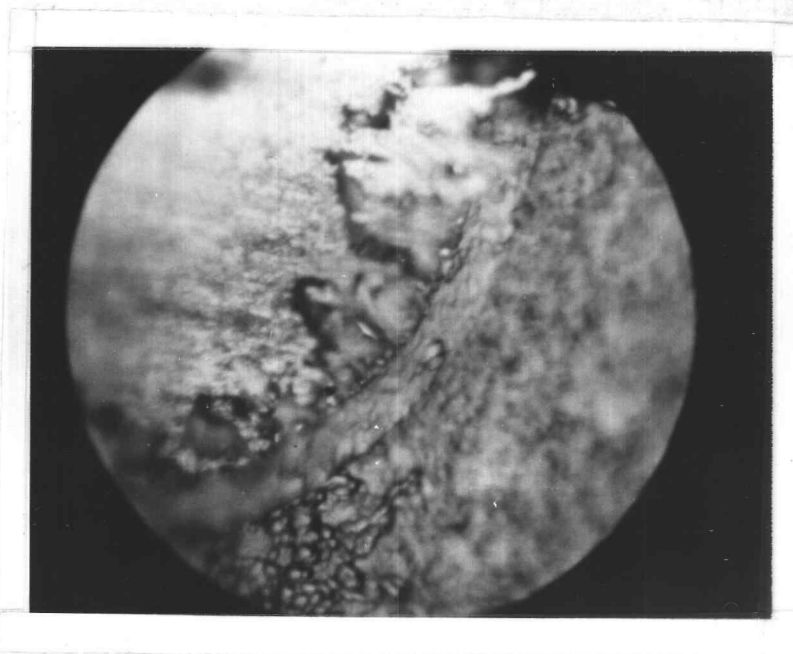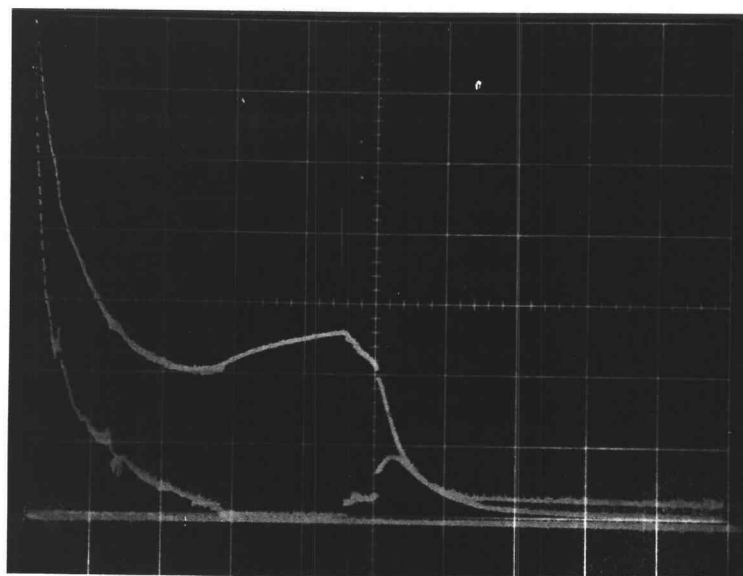In Figure 15 (a) the voltage trace drops from 120 volts (the initial capacitor voltage, not completely shown) to ten volts when arc initiates. Then the arc voltage rises to 13 volts and starts dropping again towards zero when arc extinguishes. According to the pictures taken by the author, the arc voltage is not a constant, which varies between ten volts and 20 volts, therefore the 15 volt value assumed in section II b is reasonable.

In Figure 15 (a) the current trace has a first peak, (not completely shown) which occurs at the arc initiation. The second arc current peak is due to arc extinction. There is a flat pedestal in the current trace just before the second extinction peak, which is due to molten material bridging the arc (8, p. 890).

The arc current went to zero after 1.5 milli-seconds had passed. This is probably due to wire tip shrinkage which gives an open circuit to the arc current path.

d. Junction Capacitance and Impurity Profile

All the data in Appendix IV were taken according to the procedure described in section IV d. From these data the impurity profiles of the junctions can be evaluated. Then the relation between the manufacturing process and the resulting impurity profiles of the junctions can be determined.
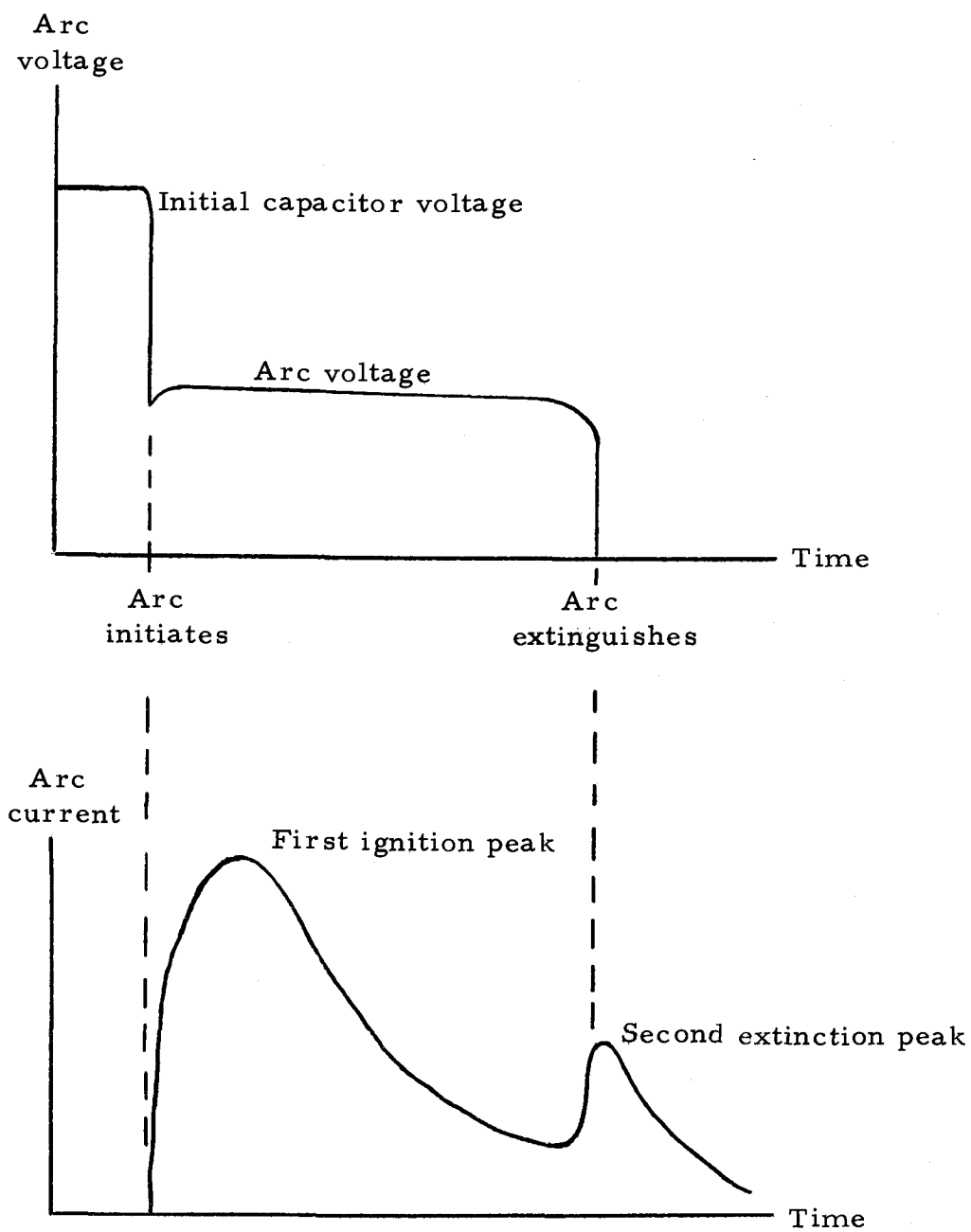
Figure 15(b).   Predicted arc voltage and arc current relation
(2, p. 59).

Two relations were used here to find the impurity profiles,

namely, (5, p. 247)

$$C = \epsilon A / W \qquad (22)$$

where:

C = junction capacitance

ϵ = semiconductor permitivity

A = junction area

W = junction depth

and (5, p. 248)

$$A^2 N(W) = \frac{2}{e\epsilon} \left[\frac{d(1/C^2)}{d(V_T)} \right]^{-1} \qquad (23)$$

where:

N(W) = impurity concentration as a function of junction depth

e = electronic charge

V_T = voltage applied to junction

= (reverse bias, V_R) + (barrier voltage, V_B)

It is assumed that the junction area   A   is a constant, its variation with respect to bias is negligible; the impurity concentration is higher on one side, the depletion layer extends only into the more lightly doped side; the impurity atoms are completely ionized at room temperature; and the applied voltage appears entirely across the

junction.

The following efforts are due to the lack of accurate values of junction area A, thus normalized values must be used instead of exact values.

From Equation (22)

$$1/C = \frac{1}{\epsilon A} \, W \qquad (24)$$

so $1/C$ is proportion to junction depth W.

Since $V_T = V_B + V_R$ and V_B is a constant, Equation (23) gives:

$$\left[\frac{d(1/C^2)}{d(V_T)}\right]^{-1} = \left[\frac{d(1/C^2)}{d(V_R)}\right]^{-1} = \frac{A^2 e\epsilon}{2} \, N(W) \qquad (25)$$

which means the inverse of the slope of $1/C^2$ versus V_R plot is proportional to impurity concentration N(W).

Figure 16 and Figure 17 are the plots of $1/C^2$ versus V_R of simple alloyed junctions and alloyed percussive-welded junctions respectively. Data from Appendix II were used.

Figure 18 and Figure 19 are the plots of $\left[\frac{d(1/C^2)}{d(V_R)}\right]^{-1}$ versus $1/C$ of simple alloyed junctions and alloyed percussive-wended junctions respectively. Since Equation (25) shows that $\left[\frac{d(1/C^2)}{d(V_R)}\right]^{-1}$ is proportional to N(W), and Equation (24) shows that $1/C$ is proportional to W, Figure 18 and Figure 19 are N(W) versus W
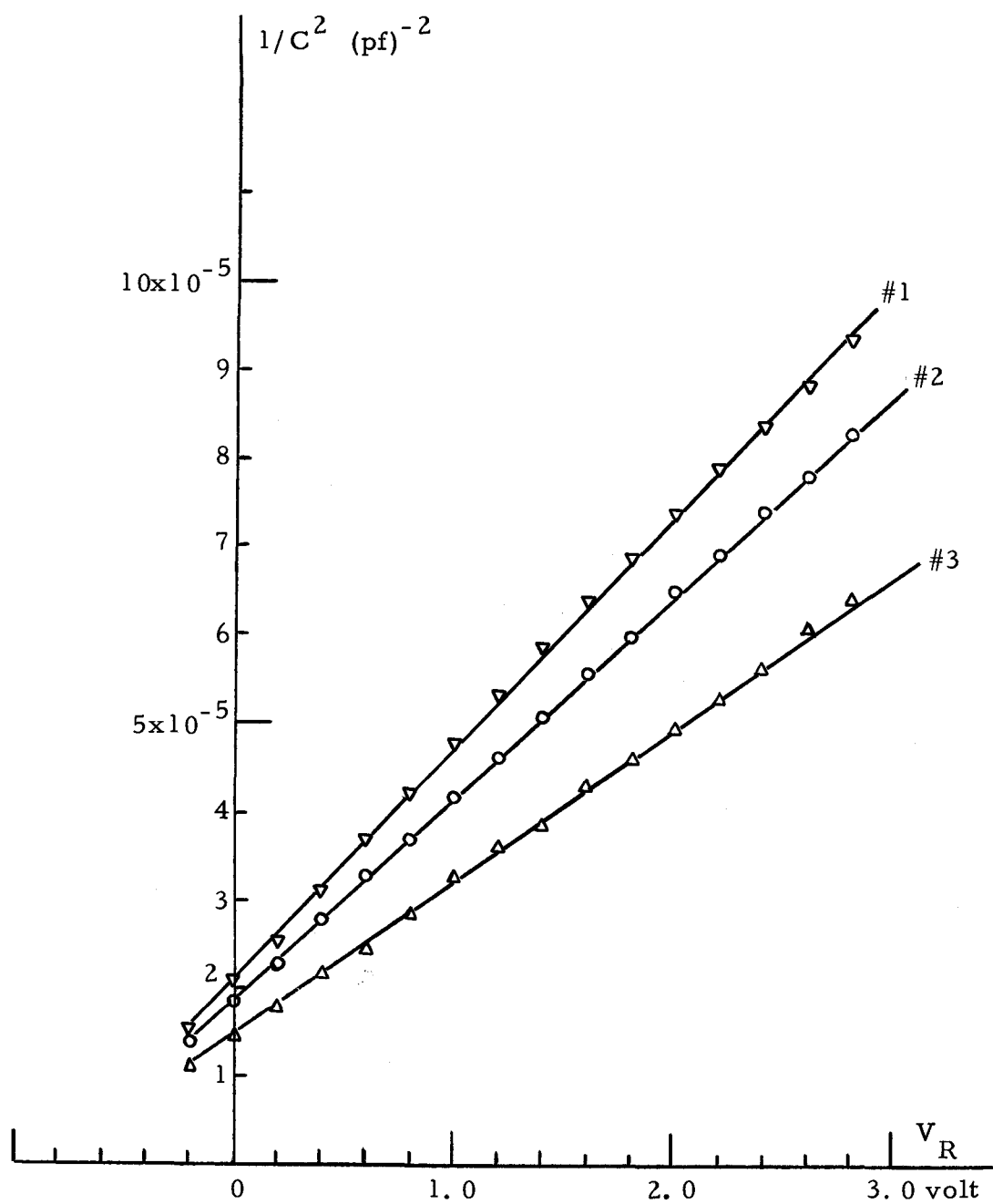
Figure 16. $1/C^2$ versus reverse bias V_R of simple alloyed junctions.
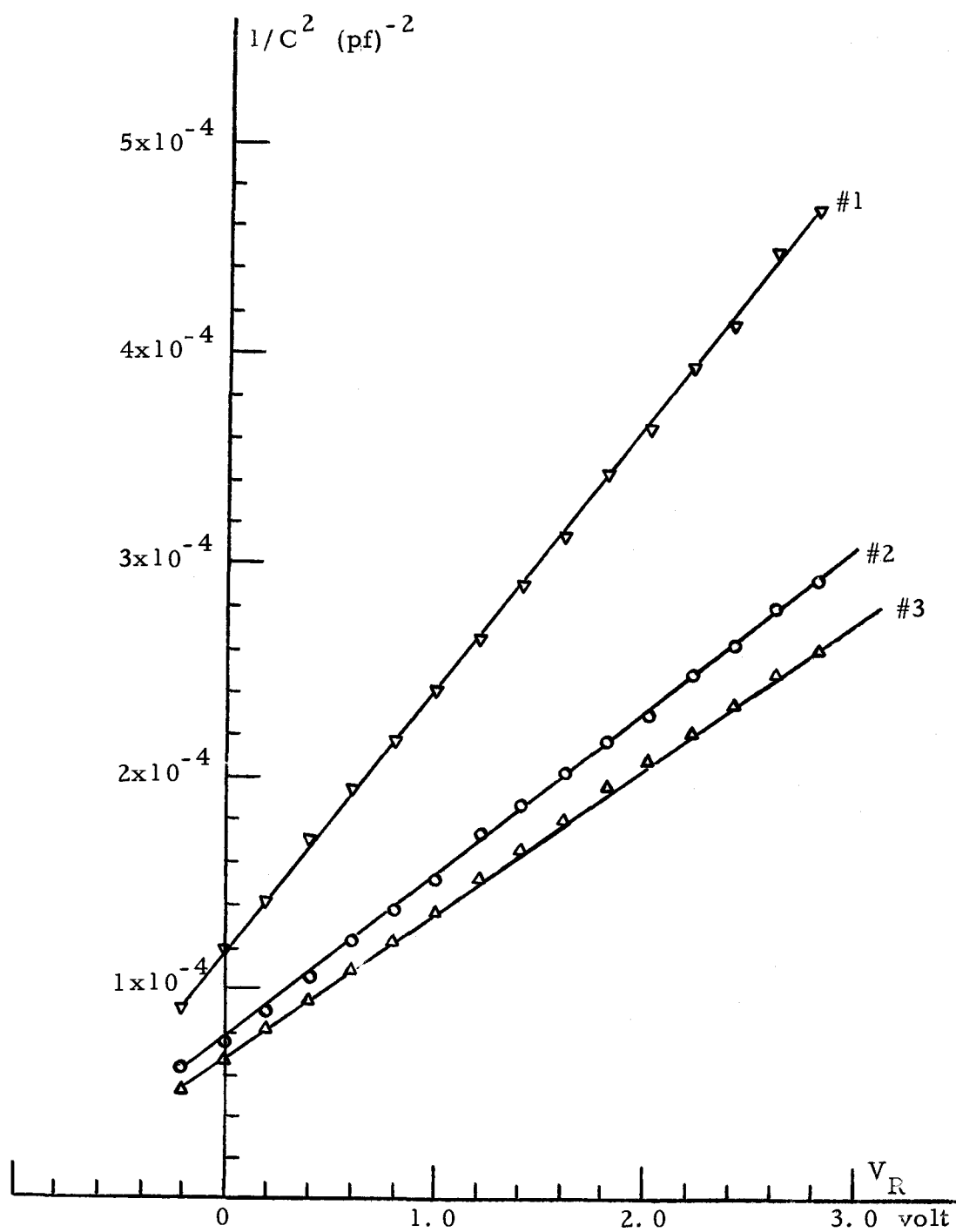
Figure 17. $1/C^2$ versus reverse bias V_R of alloyed percussive-welded junctions.
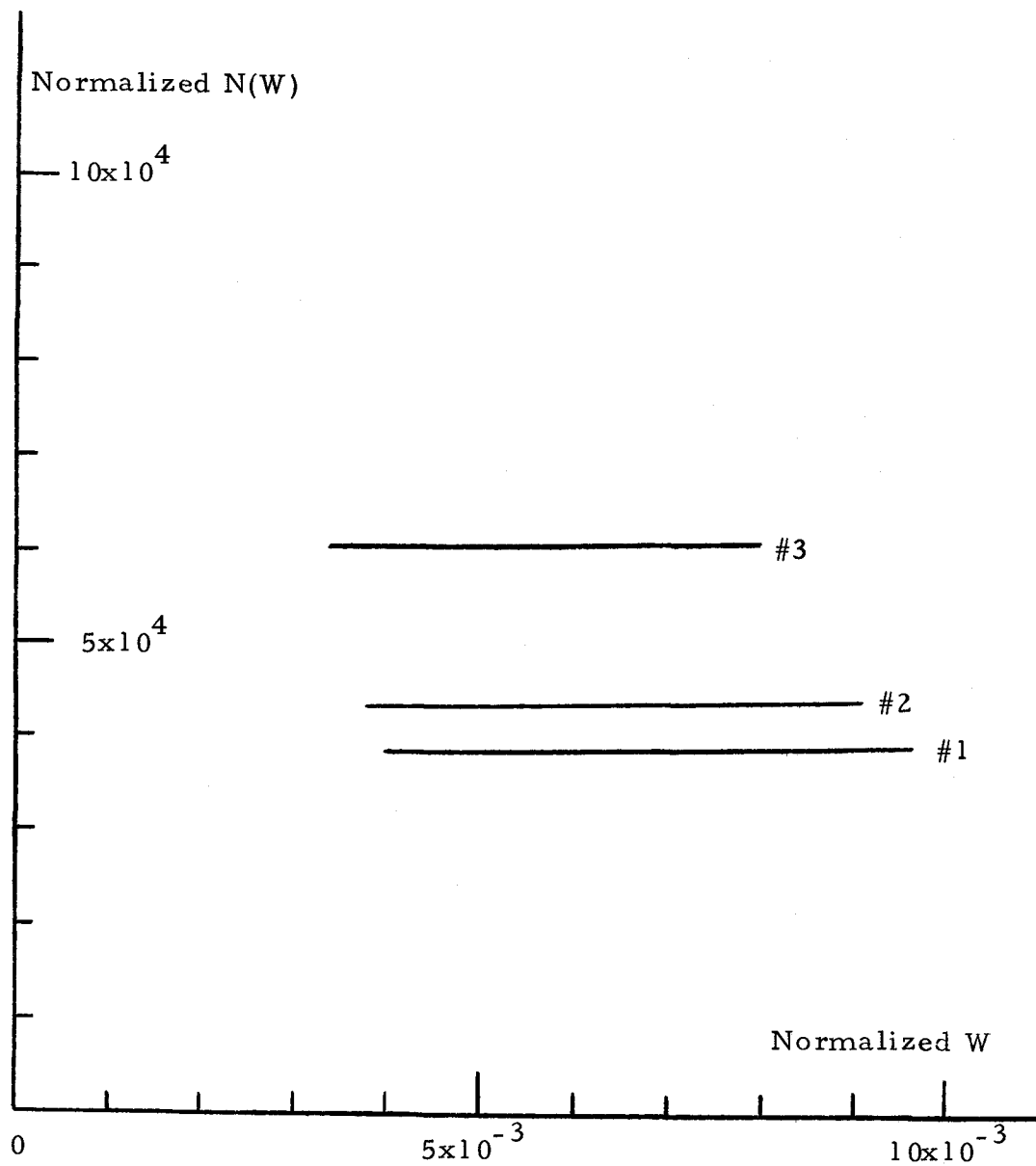
Figure 18. Impurity profiles of simple alloyed junctions.

Vertical: $[\frac{d(1/C^2)}{d(V_R)}]^{-1}$ or $\frac{A^2 e\epsilon}{2} N(W)$ in $(pf)^2(volt)$

Horizontal: $1/C$ or $\frac{1}{\epsilon A} W$ in $(pf)^{-1}$
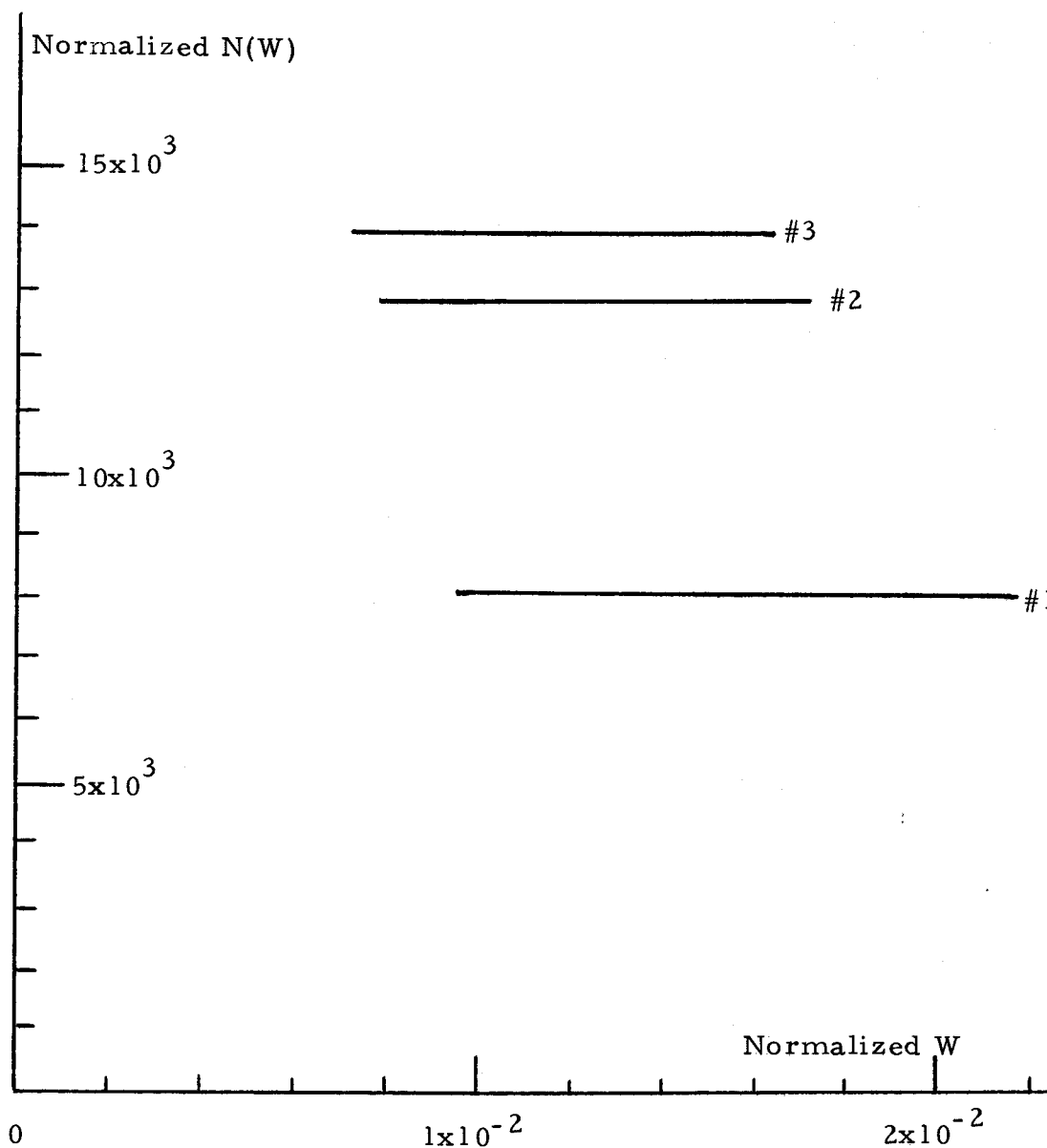
Figure 19. Impurity profiles of alloyed percussive-welded junctions.

Vertical: $[\frac{d(1/C^2)}{d(V_R)}]^{-1}$ or $\frac{A^2 e\epsilon}{2} N(W)$ in $(pf)^2(volt)$

Horizontal: $1/C$ or $\frac{1}{\epsilon A} W$ in $(pf)^{-1}$

plots, namely they are impurity profiles.

In finding $[\frac{d(1/C^2)}{d(V_R)}]^{-1}$ for the simple alloyed junction sample #1, from Figure 16 curve #1 when ΔV_R is one volt, (from one volt to two volts) $\Delta(1/C^2)$ is 2.6×10^{-5} (pf)$^{-2}$, (from 4.8×10^{-5} to 7.4×10^{-5}) so $\frac{d(1/C^2)}{d(V_R)}$ is 2.6×10^{-5} (pf)$^{-2}$(volt)$^{-1}$. And the inverse of this gives $[\frac{d(1/C^2)}{d(V_R)}]^{-1}$ to be 3.85×10^4 (pf)^2(volt). In the same way the corresponding values of other samples are found and plotted. The $1/C$ values were found in Appendix II.

The curves in **Figure 16** and **Figure 17** appear to be straight lines, but the areas of the junctions are different, so the curves have different slopes as shown in **Figure 16** and **Figure 17**.

Figure 18 and Figure 19 are horizontal lines, since these impurity profiles are the plots of the slopes of Figure 16 and Figure 17. The differences in heights of impurity profiles are due to different junction areas involved.[6]

The extrapolations of the curves in Figure 16 and Figure 17 give the estimations of the barrier voltages of the junctions, which are less than one volt. The barrier voltage can not be determined from junction capacitance measurement accurately (1, p. 282).

The impurity profiles in Figure 18 are horizontal lines the same as those in Figure 19, the former are for simple alloyed

---

[6] Refer to Equation (25).

junctions, the latter are for alloyed percussive-welded junctions,

thus it can be concluded that the alloyed percussive-welded junction

is comparable to the simple alloyed junction in impurity profile flat-

ness.

VI. SUMMARY AND CONCLUSIONS

The fabrication of P-N junctions by a percussive welding process has been studied.

The theoretical aspects of percussive welding, the requirements of a welding apparatus, the difficulty of fabricating rectifying junctions through percussive welding only, and the alloyed percussive-welded junction characteristics as compared to the simple alloyed junction have been investigated.

Experimental results and theoretical explanations of the junction characteristics were given.

It has been found necessary to add an alloying heat cycle to a percussive-welded junction, so that a rectifying junction will result. The resulting junction is comparable to a simple alloyed junction in impurity profile flatness. Since an alloying cycle is necessary, there is no advantage to using a percussive welding process over a simple alloying process.

BIBLIOGRAPHY

1. Chang , Y. F. The capacitance of P-N junctions. Solid-State Electronics 10:281-287. 1967.

2. Coyne, J. C. Monitoring the percussive welding process for attaching wires to terminals. Bell System Technical Journal 42: 55-78. 1963.

3. Hansen, Max. Constitution of binary alloys. 2d ed. New York, McGraw-Hill, 1958. 1305 p.

4. Heck, L. D. Percussive welding of metal-semiconductor contacts. Master's thesis. Corvallis, Oregon State University, 1964. 48 numb. leaves.

5. Hilibrand, J. and R. D. Gold. Determination of the impurity distribution in junction diodes from capacitance voltage measurements. RCA Review 21:245-252. 1960.

6. Kreith, Frank. Principles of heat transfer. Scranton, Internation Text Book. 1958. 553 p.

7. Oregon Research Engineers. Report on the theoretical aspects of stud welding. Corvallis, 1963. 16 numb. leaves. (Duplicated)

8. Sumner, E. E. Some fundamental problems in percussive welding. Bell System Technical Journal 33:885-895. 1954.

APPENDICES

APPENDIX I.

a. Derivations of Equation (21).
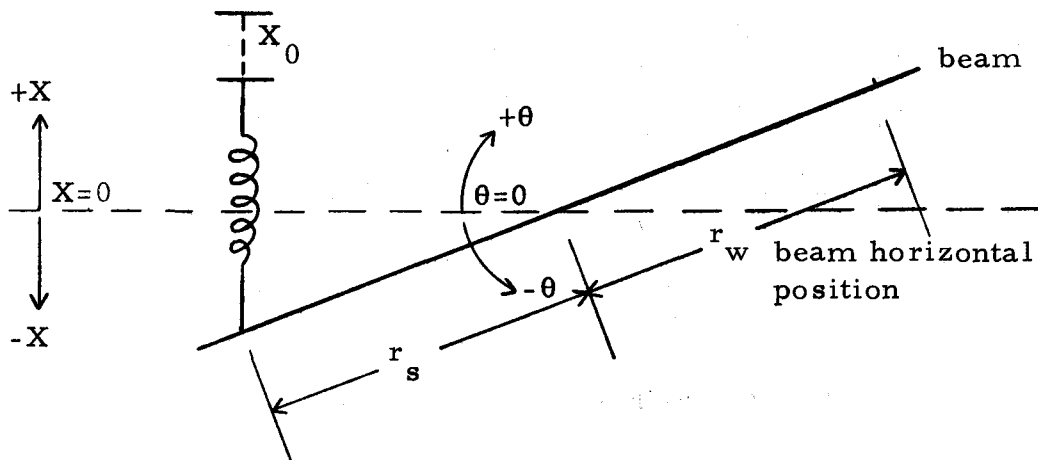
Figure I-1. Schematic diagram of beam.

Assume when the beam is in horizontal position there is no initial elongation in the spring and there is no force in the spring either. If friction is negligible, then

τ_q = torque due to spring deformation in lb-in.

$$= (\frac{K}{16} X_0 - \frac{K}{16} X) r_S \qquad (I-1)$$

where

K = spring stiffness in ounce per inch

X_0 = initial elongation of spring in inch

X = deformation of the spring in inch; positive when the left

end of beam is above horizontal; negative when the left

end of beam is below horizontal; zero when beam is

level

r_S = moment arm of spring force in inch

θ = angular displacement of beam in radian.

For a simpler differential equation obtained later, r_S is

used for $r_S \cos \theta$ for $|\theta| \leq 1/6$ radians which is the operating

range of this beam.

Assume $r_S \theta$ for X for $\theta \leq 1/6$ radian, then

$$T_q = (\frac{K}{16} X_0 - \frac{K}{16} r_S \theta) r_S \qquad (I-2)$$

but:

$$T_q = I \alpha = I \frac{d^2\theta}{dt^2} \qquad (I-3)$$

where:

I = moment of inertia of beam in slug-in.^{2}

α = angular acceleration of beam

$= \frac{d^2\theta}{dt^2}$ in radian/sec.^{2}.

so

$$(\frac{K}{16} X_0 - \frac{K}{16} r_S \theta) r_S = I \frac{d^2\theta}{dt^2} \qquad (I-4)$$

or

$$\frac{d^2\theta}{dt^2} + \frac{r_S^2 K}{16I}\theta = \frac{KX_0 r_S}{16I} \tag{I-5}$$

then the solution should be:

$$\theta = C_1 e^{i\frac{r_S}{4}\sqrt{\frac{K}{I}}t} + C_2 e^{-i\frac{r_S}{4}\sqrt{\frac{K}{I}}t} + \frac{X_0}{r_S} \tag{I-6}$$

with initial conditions:

$$\theta(0) = -\theta_0 \tag{I-7}$$

$$\theta'(0) = \frac{d\theta}{dt}\Big|_{t=0}$$

$$= \text{initial angular velocity of beam}$$

$$= 0 \tag{I-8}$$

Thus

$$-\theta_0 = C_1 + C_2 + \frac{X_0}{r_S} \tag{I-9}$$

$$0 = C_1 i \frac{r_S}{4}\sqrt{\frac{K}{I}} - C_2 i \frac{r_S}{4}\sqrt{\frac{K}{I}} \tag{I-10}$$

Solving the simultaneous equations above will give

$$C_1 = C_2 = -\frac{1}{2}(\theta_0 + \frac{X_0}{r_S}) \tag{I-11}$$

Equation (I-6) will then give

$$\theta = -\frac{1}{2}(\theta_0 + \frac{X_0}{r_S})\left[e^{i\frac{r_S}{4}\sqrt{\frac{K}{I}}t} + e^{-i\frac{r_S}{4}\sqrt{\frac{K}{I}}t}\right] + \frac{X_0}{r_S}$$

$$= -(\theta_0 + \frac{X_0}{r_S})\left[\cos\left(\frac{r_S}{4}\sqrt{\frac{K}{I}}t\right)\right] + \frac{X_0}{r_S} \qquad (I-12)$$

but

$$\omega = \text{angular velocity of beam}$$

$$= \frac{d\theta}{dt}$$

$$= (\theta_0 + \frac{X_0}{r_S})(\frac{r_S}{4}\sqrt{\frac{K}{I}}) \sin\left(\frac{r_S}{4}\sqrt{\frac{K}{I}}t\right) \qquad (I-13)$$

From Equation (I-12), if $\theta = 0$ when the beam is horizontal in position again, then

$$\cos\left(\frac{r_S}{4}\sqrt{\frac{K}{I}}t\right) = \frac{\dfrac{X_0}{r_S}}{\theta_0 + \dfrac{X_0}{r_S}} = \frac{X_0}{\theta_0 r_S + X_0}$$

$$\sin\left(\frac{r_S}{4}\sqrt{\frac{K}{I}}t\right) = \sqrt{1 - \left(\frac{X_0}{\theta_0 r_S + X_0}\right)^2}$$

at that instant, ω is ω_f (final angular velocity of the beam) and Equation (I-13) will give

$$\omega_f = (\theta_0 + \frac{X_0}{r_S})(\frac{r_S}{4}\sqrt{\frac{K}{I}})\sqrt{1 - (\frac{X_0}{\theta_0 r_S + X_0})^2}$$

$$= \frac{1}{4}\sqrt{\frac{K}{I}}\sqrt{\theta_0 r_S (2X_0 + \theta_0 r_S)} \qquad (I-14)$$

but

$$\omega_f = \frac{V_{wf}}{r_w} \qquad (I-15)$$

where:

V_{wf} = wire tip final approaching speed in inch per second

r_w = radius of rotation of wire tip in inch.

thus Equation (I-14) will lead to

$$\frac{V_{wf}}{r_w} = \frac{1}{4}\sqrt{\frac{K}{I}}\sqrt{\theta_0 r_S (2X_0 + \theta_0 r_S)} \qquad (I-16)$$

b. Moment of Inerita of Main Beam
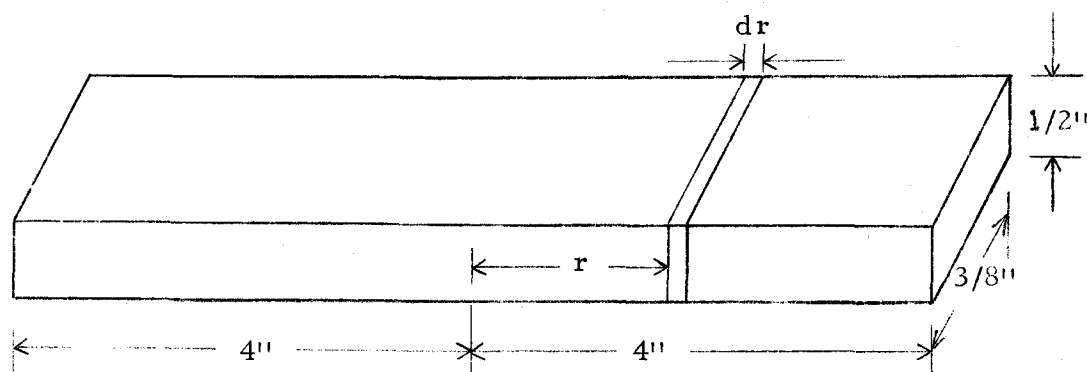
Figure I-2. The beam. (Not to scale)

dI = differential moment of inertia of beam

$$= dm \; r^2$$

$$= D_{Al} \, (dr) \, (1/2) \, (3/8) \, r^2 \qquad \text{(I-17)}$$

where:

D_{Al} = density of aluminum

$$= 2.7 \; gm/cm^3 = 0.0976/32.2 \; slug/in^3$$

I = moment of inertia of beam

$$I = \int dI = \int_{-4}^{4} (0.0976/32.2)(1/2)(3/8)r^2 \, dr = 0.0242 \; slug\text{-}in^2$$

$$\text{(I-18)}$$

APPENDIX II

Junction Capacitances Versus Bias Voltages Data

a. Simple alloyed junction sample #1

V_T volt	V_R volt	C (pf)	$1/C$ $(pf)^{-1}$	$1/C^2$ $(pf)^{-2}$
$2.8 + V_B$	2.8	103.3	9.68×10^{-3}	0.35×10^{-5}
$2.6 + V_B$	2.6	106.3	9.40	8.82
$2.4 + V_B$	2.4	109.4	9.14	8.33
$2.2 + V_B$	2.2	112.6	8.90	7.90
$2.0 + V_B$	2.0	116.4	8.60	7.40
$1.8 + V_B$	1.8	120.3	8.30	6.90
$1.6 + V_B$	1.6	125.0	8.00	6.40
$1.4 + V_B$	1.4	130.0	7.70	5.90
$1.2 + V_B$	1.2	136.6	7.33	5.38
$1.0 + V_B$	1.0	144.2	6.94	4.80
$0.8 + V_B$	0.8	153.2	6.53	4.25
$0.6 + V_B$	0.6	164.2	6.09	3.70
$0.4 + V_B$	0.4	179.0	5.59	3.12
$0.2 + V_B$	0.2	200.0	5.00	2.50
$0 + V_B$	0.	219.4	4.56	2.08
$-0.2 + V_B$	-0.2	253.8	3.94	1.55

b. Simple alloyed junction sample #2

V_T volt	V_R volt	C (pf)	$1/C$ (pf)$^{-1}$	$1/C^2$ (pf)$^{-2}$
$2.8 + V_B$	2.8	110.0	9.10×10^{-3}	8.30×10^{-5}
$2.6 + V_B$	2.6	113.2	8.83	7.80
$2.4 + V_B$	2.4	116.2	8.61	7.40
$2.2 + V_B$	2.2	120.4	8.31	6.90
$2.0 + V_B$	2.0	124.1	8.06	6.50
$1.8 + V_B$	1.8	129.2	7.75	6.00
$1.6 + V_B$	1.6	133.7	7.48	5.60
$1.4 + V_B$	1.4	140.3	7.15	5.10
$1.2 + V_B$	1.2	146.8	6.82	4.65
$1.0 + V_B$	1.0	154.2	6.49	4.20
$0.8 + V_B$	0.8	164.3	6.08	3.70
$0.6 + V_B$	0.6	174.1	5.75	3.30
$0.4 + V_B$	0.4	189.0	5.29	2.80
$0.2 + V_B$	0.2	208.2	4.80	2.30
$0 \;\;\; + V_B$	0	228.5	4.36	1.90
$-0.2 + V_B$	-0.2	267.4	3.74	1.40

c. Simple alloyed junction sample #3

V_T volt	V_R volt	C (pf)	$1/C$ $(pf)^{-1}$	$1/C^2$ $(pf)^{-2}$
$2.8 + V_B$	2.8	125.2	8.00×10^{-3}	6.40×10^{-5}
$2.6 + V_B$	2.6	128.6	7.78	6.05
$2.4 + V_B$	2.4	133.8	7.48	5.60
$2.2 + V_B$	2.2	137.8	7.26	5.28
$2.0 + V_B$	2.0	142.9	7.01	4.90
$1.8 + V_B$	1.8	147.5	6.78	4.60
$1.6 + V_B$	1.6	152.8	6.55	4.30
$1.4 + V_B$	1.4	161.1	6.20	3.85
$1.2 + V_B$	1.2	166.8	6.00	3.60
$1.0 + V_B$	1.0	175.5	5.70	3.25
$0.8 + V_B$	0.8	189.0	5.29	2.80
$0.6 + V_B$	0.6	202.1	4.95	2.45
$0.4 + V_B$	0.4	215.8	4.64	2.15
$0.2 + V_B$	0.2	239.2	4.18	1.75
$0 \ + V_B$	0	267.3	3.74	1.40
$-0.2 + V_B$	-0.2	301.5	3.32	1.10

d. Alloyed percussive-welded junction sample #1

V_T volt	V_R volt	C (pf)	$1/C$ $(pf)^{-1}$	$1/C^2$ $(pf)^{-2}$
$2.8 + V_B$	2.8	46.1	2.17×10^{-2}	4.70×10^{-4}
$2.6 + V_B$	2.6	47.2	2.12	4.49
$2.4 + V_B$	2.4	48.9	2.04	4.15
$2.2 + V_B$	2.2	50.3	1.99	3.95
$2.0 + V_B$	2.0	52.2	1.915	3.65
$1.8 + V_B$	1.8	53.9	1.86	3.45
$1.6 + V_B$	1.6	56.1	1.78	3.16
$1.4 + V_B$	1.4	58.5	1.71	2.92
$1.2 + V_B$	1.2	61.2	1.635	2.66
$1.0 + V_B$	1.0	64.4	1.555	2.41
$0.8 + V_B$	0.8	67.7	1.48	2.18
$0.6 + V_B$	0.6	71.7	1.395	1.94
$0.4 + V_B$	0.4	76.4	1.31	1.71
$0.2 + V_B$	0.2	83.7	1.195	1.42
$0 + V_B$	0	91.8	1.09	1.18
$-0.2 + V_B$	-0.2	105.0	0.95	0.90

e. Alloyed percussive-welded junction sample #2

V_T volt	V_R volt	C (pf)	$1/C$ $(pf)^{-1}$	$1/C^2$ $(pf)^{-2}$
$2.8 + V_B$	2.8	58.25	1.718×10^{-2}	2.95×10^{-4}
$2.6 + V_B$	2.6	59.80	1.672	2.80
$2.4 + V_B$	2.4	61.61	1.622	2.63
$2.2 + V_B$	2.2	63.50	1.575	2.48
$2.0 + V_B$	2.0	66.00	1.517	2.30
$1.8 + V_B$	1.8	67.82	1.478	2.18
$1.6 + V_B$	1.6	70.30	1.421	2.02
$1.4 + V_B$	1.4	73.15	1.368	1.87
$1.2 + V_B$	1.2	75.60	1.321	1.75
$1.0 + V_B$	1.0	81.11	1.232	1.52
$0.8 + V_B$	0.8	85.75	1.168	1.36
$0.6 + V_B$	0.6	90.50	1.105	1.22
$0.4 + V_B$	0.4	97.80	1.024	1.05
$0.2 + V_B$	0.2	105.5	0.949	0.90
$0 \quad + V_B$	0	115.6	0.865	0.75
$-0.2 + V_B$	-0.2	127.0	0.787	0.62

f. Alloyed percussive-welded junction sample #3

V_T volt	V_R volt	C (pf)	$1/C$ (pf)$^{-1}$	$1/C^2$ (pf)$^{-2}$
$2.8 + V_B$	2.8	61.80	1.620×10^{-2}	2.62×10^{-4}
$2.6 + V_B$	2.6	63.46	1.578	2.49
$2.4 + V_B$	2.4	65.12	1.537	2.36
$2.2 + V_B$	2.2	67.11	1.490	2.22
$2.0 + V_B$	2.0	69.40	1.442	2.08
$1.8 + V_B$	1.8	71.52	1.400	1.96
$1.6 + V_B$	1.6	74.50	1.342	1.80
$1.4 + V_B$	1.4	77.91	1.285	1.65
$1.2 + V_B$	1.2	81.13	1.232	1.52
$1.0 + V_B$	1.0	85.80	1.167	1.36
$0.8 + V_B$	0.8	90.51	1.105	1.22
$0.6 + V_B$	0.6	96.21	1.040	1.08
$0.4 + V_B$	0.4	103.1	0.970	0.94
$0.2 + V_B$	0.2	112.0	0.894	0.80
$0 + V_B$	0	124.1	0.806	0.65
$-0.2 + V_B$	-0.2	138.8	0.721	0.52